Intramural Mechanics in the Human Tongue

by

Vitaly J. Napadow

B.S. Mechanical Engineering
Cornell University, 1995

SUBMITTED TO THE DEPARTMENT OF MECHANICAL ENGINEERING IN PARTIAL FULFILLMENT OF THE REQUIREMENTS FOR THE DEGREE OF

MASTER OF SCIENCE IN MECHANICAL ENGINEERING
AT THE
MASSACHUSETTS INSTITUTE OF TECHNOLOGY

JUNE 1998

Signature of Author:

Department of Mechanical Engineering
May 25, 1998

Certified By:

Richard J. Gilbert, M.D.
Department of Mechanical Engineering
Thesis Supervisor

Certified By:

Rohan Abeyaratne
Professor of Mechanical Engineering
Co-Thesis Advisor

Accepted By:

Ain A. Sonin
Professor of Mechanical Engineering
Chairman, Graduate Committee

Intramural Mechanics in the Human Tongue

By

Vitaly J. Napadow

Submitted to the Department of Mechanical Engineering
On May 25th 1998 in Partial Fulfillment of the Requirements
for the Degree of Master of Science in Mechanical Engineering

Abstract

Contraction of the tongue musculature during physiological motions (anterior protrusion, sagittal bending, swallowing) is associated with characteristic patterns of tissue deformation. Coupling knowledge of this tissue deformation with the underlying myoarchitecture offers the ability to explore complex structure-function relationships in the organ. In order to quantify strain in the human tongue, a non-invasive MRI tagging technique was used in combination with a fast asymmetric gradient echo imaging pulse sequence (TurboFLASH). This MRI technique discretized tissue into non-linear deforming elements. Individual elements were defined by selectively supersaturating bands of magnetic spins in resting tongue tissue along the antero-posterior and superior-inferior directions of the mid-sagittal plane, resulting in a rectilinear square grid. Axial and shear strains relative to the rest condition were determined for each element and represented by two-dimensional surface strain maps. Tongue myoarchitecture was studied with diffusion-tensor MRI. A slice select pulsed gradient stimulated echo pulse sequence was applied to derive the spatial diffusion tensor field in the tongue. Tensor eigenvectors and measures of anisotropy were used to derive a virtual anatomical atlas of the bovine tongue. During forward protrusion, the anterior tongue underwent positive antero-posterior strain (elongation) and symmetrical negative medial-lateral and superior-inferior strain (contraction). During sagittal bending directed to the hard palate, the tongue exhibited positive asymmetrical antero-posterior strain that increased radially as a function of distance from the center of curvature, with commensurate negative strain in the medial-lateral direction. Similarly, the magnitude of anterior-posterior strain during left-directed tongue bending was proportional to distance from the curved inner surface. The oral stage of the swallow was subdivided into an early accommodative phase, a late accommodative phase and a propulsive phase. For bolus accommodation, strain findings were consistent with contraction of the anteriorly located intrinsic muscles and the posteriorly located genioglossus and hyoglossus muscles. For bolus propulsion, strain findings were consistent with posterior passive stretch in the midline due to contractions of the laterally inserted styloglossus muscle, as well as contraction of posteriorly located intrinsic muscles. In conclusion, regulation of tongue deformation was related to regional activation of intrinsic and/or extrinsic lingual musculature, which was appreciated with 3D diffusion tensor visualization.

Thesis Supervisor: Richard J Gilbert, M.D.
Title: Lecturer Department of Mechanical Engineering

Acknowledgements

There were many people who contributed both personally and scientifically to this thesis and I would like to offer my sincere thanks for their generous assistance. My advisor, Dr. Richard Gilbert, has provided continued support for this project as well as for my own personal academic growth. His patience, respect, and unceasing optimism have helped keep the spark of interest for this project alive over the past two years and I would like to thank him for his substantial academic and financial contributions to this thesis. I would also like to thank Dr. Van Wedeen for our lively conversations on topics ranging from mechanics and MRI to meat slicers and super-tensors. I would like to acknowledge Dr. Rohan Abeyaratne for his very generous availability and support in all matters of engineering, and Dr. Qun Chen for his assistance in the development of the magnetic resonance methodology and patience with my still expanding foray into the wonderful world of magnetic resonance imaging. Finally, I would like to thank the Whitaker Foundation whose generous financial support has helped me continue my graduate education and has kept my rent checks from bouncing.

Table of Contents

List of Figures

List of Tables

1 Introduction

The human tongue is a complex muscular organ that is of paramount importance for many physiological tasks including deglutition (swallowing) and phonation (speech). The tongue is classified as a muscular hydrostat, that is, an organ whose musculature both creates motion and supplies skeletal support for that motion. It capitalizes on its high water content, and hence incompressibility, to quickly and efficiently alter its form while maintaining its original volume. For example, concavities in the tongue can be created by direct tissue contraction, whereas convexities (bulging regions) can be created by tissue expansion along directions orthogonal to muscle fiber contraction.

The tongue can be considered analogous to other muscular hydrostats, such as the elephant trunk and squid tentacle, which are composed almost entirely of muscle and devoid of any calcified internal or external skeletal elements (Smith and Kier, 1989). All possess regions of fibers parallel and perpendicular to the organ's long axis, but differ regarding the relative position and geometry of the perpendicular fibers. That is, perpendicular fibers can be present at the tissue's long axis or peripheral to it, at the expense of the longitudinal fibers. Muscular hydrostats that perform significant bending functions tend to have longitudinal fibers situated away from the long axis, thereby producing greater bending moments about this axis. This arrangement is seen in the tongues of many animals, including the snake, which flicks its chemoreceptor-laden organ to sense its prey. The elephant trunk is highly adaptive, and has fibers that spiral down its long axis on the tissue's periphery, thus maximizing its ability to perform torsional deformations, such as in grasping arboreal vegetation. Furthermore, all of these organs use their musculature to not only produce deformation, but also to provide rigidity and thus skeletal support for this deformation. These types of structure/function relationships have been explored in this thesis for the case of the human tongue.

1.1 Magnetic Resonance Imaging

Nuclear Magnetic Resonance (NMR) or Magnetic Resonance Imaging (MRI - the nomenclature employed in the clinical medicine world to avoid the connotations of

"nuclear" in NMR), was an integral technology employed in this study. This brief introduction into MRI is not intended to be an all encompassing discourse of the technology's classical or quantum mechanics phenomena; however, some background is in order and will be provided.

MRI employs energy in the radio frequency (RF) band of the electromagnetic spectrum; coupled with static magnetic fields with strengths on the order of a Tesla (the magnet used was a 1.5T Siemens Vision System). The magnetic resonance phenomenon exists only for nuclei with non-zero spin quantum numbers, I, which denotes an odd number of protons or neutrons. Hydrogen, ^1H, satisfies this condition, having a spin quantum number equal to ½. Furthermore, this element is ubiquitous in the human body, which is composed mainly (70%) of water, H_2O, thus providing ample resource to study this phenomenon. Due to its non-zero spin quantum number, hydrogen has an induced nuclear magnetic moment,

$$\mu = \gamma_H \hbar I \tag{1.0}$$

where γ_H = 42.6MHz/T is the proton (^1H) gyromagnetic ratio and $\hbar$ is Plank's constant. The proton acts as a magnetic dipole, alternating between its positive and negative spin states. In the presence of an external magnetic field, B_0, ^1H experiences an interaction energy given by

$$E = \vec{\mu} \bullet \vec{B}_0 \tag{2.0}$$

For I = ½ nuclei, there exist two allowable states for the magnetic moment to align with the external magnetic field, parallel and anti-parallel. The interaction energy increases with the strength of the external field, as does the energy difference, ΔE, between the parallel and anti-parallel aligned dipoles (Figure 1).

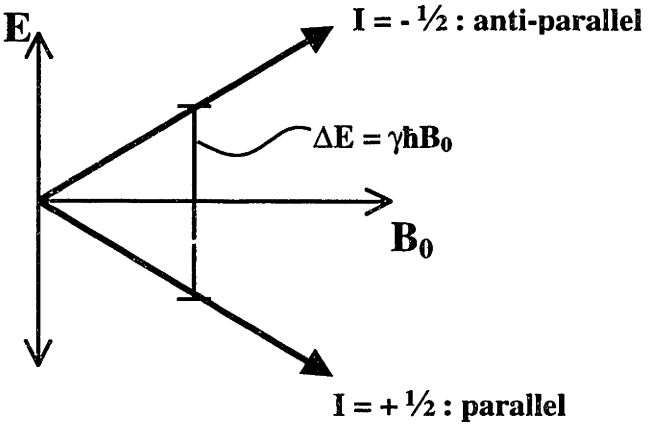

Figure 1 - Energy associated with the interaction of the proton magnetic dipole and an external magnetic field. There are two allowable states for the dipole, parallel and anti-parallel with B_0.

Spins prefer the lower energy state, and so will tend to align parallel with the external field. Statistically speaking, the ratio of spins aligning anti-parallel to those aligning parallel follows the Boltzmann distribution, given by

$$\frac{N_-}{N_+} = \exp\left(-\frac{\Delta E}{kT}\right) \tag{3.0}$$

where k is the Boltzmann constant and T is temperature. This spin population difference is what leads to the NMR signal.

For an observable signal to exist, there must be 10^{18} more spins aligned parallel than anti-parallel to B_0. At room temperature and at a field strength of 1.5T, the number of excess spins (parallel spins not paired with a neighboring anti-parallel spin) is only 1 in 10^5. However, in only 1ml of H_20, there are $6.7x10^{22}$ spins. Even the miniscule ratio of $1:10^5$ leads to $6.7x10^{17}$ excess parallel spins in only 1 ml of H_20. This plethora of spins provides ample signal for an NMR experiment on human tissue, which is by nature aqueous.

All of the magnetic dipoles can be represented by a single bulk sum magnetization vector,

$$\vec{M} = \sum \vec{\mu} \tag{4.0}$$

which traverses the space represented by a cone standing on end. The cone's long axis represents the external magnetic field, B_0, and the magnetization vector precesses about this axis (thus producing the cone). The Precession rate is given by the Larmor frequency,

$$\omega_0 = \gamma_H B_0 \tag{5.0}$$

In order to perform NMR experiments, energy must be input at or near the proton's Larmor frequency, ω_0. This restriction means that RF energy must be input at 1.5T, since the Larmor frequency of hydrogen at this field strength is 63.9MHz, right in the FM RF band, which stretches from 88 to 108 MHz.

In a reference frame rotating with the Larmor frequency about the B_0 axis (z-axis), the bulk magnetization vector, M_0, is stationary, and aligned with the z-axis. Spin dynamics are then governed by the famous Bloch equations (Bloch, 1946), which in vector form are

$$\frac{\mathrm{d}}{\mathrm{dt}}\vec{M}(t) = \gamma_H \vec{M}(t) \times \vec{B} - \frac{1}{T_1}(M_z - M_0)\hat{z} - \frac{1}{T_2}\left(M_x\hat{x} - M_y\hat{y}\right) \tag{6.0}$$

where M_z is amount of magnetization along the z-axis, and is termed longitudinal magnetization. M_x and M_y represent the amount of magnetization along the x and y axes respectively, and in vector sum are referred to as the transverse magnetization. Transverse magnetization is measured by the current it induces in an RF receive coil and corresponds directly to pixel intensity.

In a typical MRI experiment, short RF pulses (t=1ms) create a magnetic field, B_1, oscillating at the resonance (Larmor) frequency (that is, stationary in the rotating reference frame) which serves to tip the magnetization vector off of its equilibrium along the z-axis. Once this RF pulse has been turned off, The transverse magnetization relaxes back to nil exponentially at a rate given by a decay time constant T_2, which is an inherent property of the tissue. Simultaneously, the longitudinal magnetization relaxes back to its original value, M_0, with time constant T_1. Different tissues have different time constants, and it is this difference which provides the contrast in a typical MR image.

The imaging methodology was based on these principles of the magnetic resonance phenomena. Specific experimental details that describe the RF pulse sequences employed, will be included in the methodology sections.

1.2 Myoarchitecture

A study of lingual mechanics must incorporate the underlying 3D myoarchitecture, which is a complex array of interdigitating fibers, responsible for the tongue's almost limitless array of displacements and deformations. The human tongue is an integrated organ composed of both intrinsic fibers, i.e. those which possess no direct connection to bony surfaces, and extrinsic fibers, i.e. those which do possess connections to bony surfaces (Figure 2).

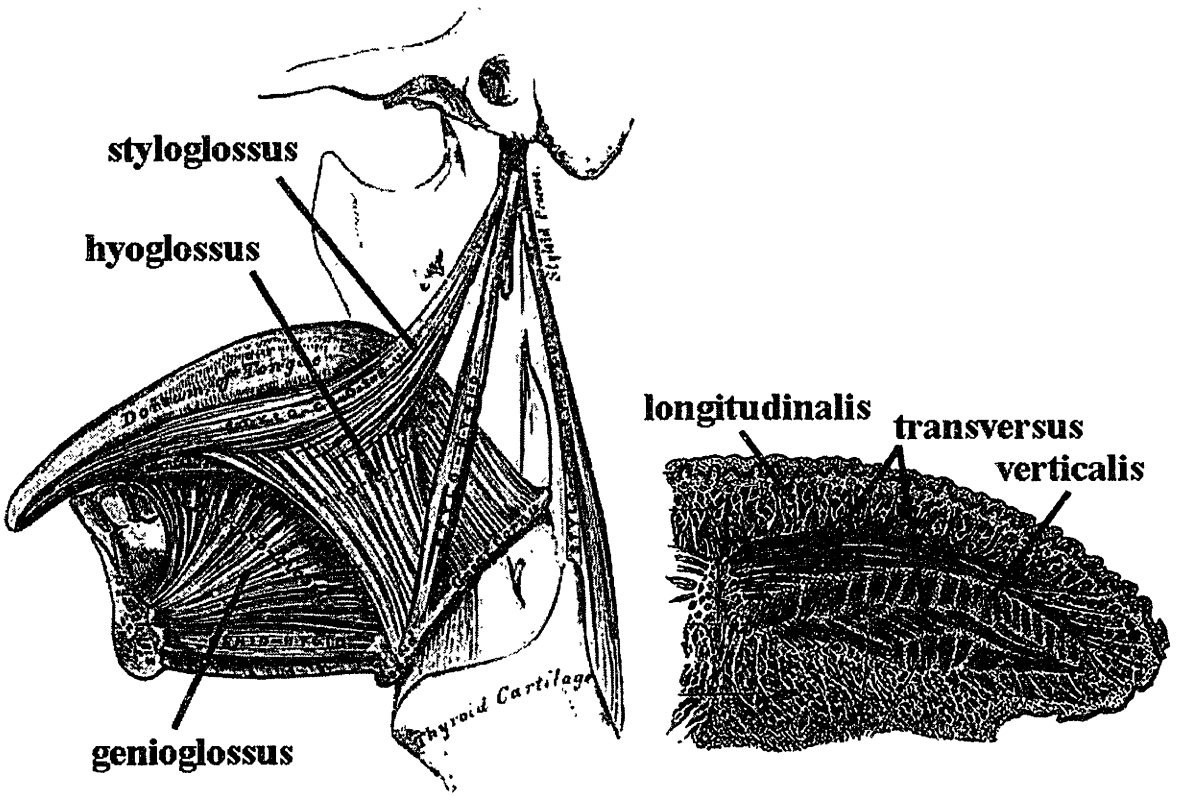

Figure 2 - Anatomy of the tongue: (Left) extrinsic muscle fibers (sagittal view) and (Right) intrinsic muscle fibers in anterior tongue (half of cross section). [Gray's Anatomy by Henry Gray. Crown Publishers, Inc., 1976]

The myoarchitecture of the anterior tongue is broadly characterized by a core region of orthogonally related muscle fibers directed medial-lateral (transversus) and superior-inferior (verticalis), contained within a sheath-like tract of longitudinally, or anterior-posterior, oriented fibers (longitudinalis). However, these populations of fibers are not ideally compartmentalized, but rather are interdigitated in a complex manner.

Furthermore, the intrinsic fibers are merged with other, extrinsic muscles originating outside the tongue proper, whose function is to modify tongue shape and position from a superior direction (palatoglossus), postero-superior direction (styloglossus), and inferior direction (genioglossus and hyoglossus). The genioglossus is a notably large muscle that originates at the mental spine of the mandible and enters the tongue from below, in a fan-like projection, comprising a considerable portion of the posterior half of the organ.

Due to the complex three-dimensional myoarchitecture of the tongue, deriving accurate information regarding muscle fiber orientation from meticulous dissection (Miyawaki, 1973) or multi-slice histology (the gold standard), an inherently two-dimensional technique, is both laborious and ill-posed. The latter problem stems from the inability of histology to resolve through plane fiber angle deviation. Furthermore, histology is rather invasive, requiring the sacrifice of the sample. When studying human subjects *in-vivo*, this particular characteristic is rather prohibitive, and necessitates a different, less invasive methodology. Addressing all of these concerns, the three-dimensional myoarchitecture of the tongue was derived in this thesis by measuring the spatially variant proton self-diffusivity with a diffusion-tensor Magnetic Resonance Imaging technique, which measures diffusivity as signal attenuation. Diffusion in muscle tissue is greatest along the fiber direction due to myofiber geometry, since cellular membranes of the cylindrically symmetric, elongated myocytes impose barriers for the self-diffusion of free water. Signal attenuation receives contributions from both intracellular and extracellular fluid; however, the elongated geometry of muscle cells insures that both components induce maximal attenuation along the myofiber long axis (Norris and Niendorf, 1995). Thus visualization of the self-diffusion tensor field can be utilized as a virtual 3D anatomical atlas of *in-vivo* muscle tissue (Basser *et al*, 1994). This technique is both non-invasive and capable of deriving full three-dimensional fiber angle orientations. In this thesis, the technique was successfully applied to an *ex-vivo* mammalian (bovine) tongue, and progress is currently being made to complete human *in-vivo* diffusion-tensor imaging.

1.3 Physiology

In deglutition, the tongue acts to contain and propel a bolus of food, whereas in phonation, the tongue assumes stereotyped conformations that determine vocal tract shape. The determination of tongue mechanics associated with these physiological functions requires an analysis of internal muscular dynamics. Previous studies of tongue mechanics have utilized photographic observation (Abd-el-Malek, 1955), video-fluoroscopy (Cook *et al*, 1989; Dodds *et al*, 1990; Kahrilas *et al*, 1992), video-fluoroscopy with ultrafast CT (Kahrilas *et al*, 1993), sonography (Hamlet *et al*, 1988; Shawker *et al*, 1984; Stone *et al*, 1990; Wein *et al*, 1991), or magnetic resonance imaging (Gilbert *et al*, 1997) to determine tongue contour and to theorize about the underlying muscular activitv. However, due to the redundancy of muscular elements found in the tongue, it is difficult to determine internal contraction patterns solely through measures of external shape. This critical point was the motivation for the current research effort.

To address this issue, various methods have been developed in the past to resolve internal tissue deformation, although each has limitations. Finite element modeling has successfully portrayed the theoretical internal mechanics of the tongue, but has been compromised by difficulties in setting valid optimization functions and incorporating the proper anatomy (Hashimoto and Suga, 1986; Wilhelms-Tricarico, 1994; Sanguineti *et al*, 1997). Similarly, attempts using simplified geometrical analog modeling have provided only a global understanding of tissue physiology (Chiel *et al*, 1992). Past empirical methods have been limited by inadequate temporal or spatial resolution. For example, studies exploring tongue deformation with fluoroscopy and implanted metal markers (surgical wire or injected solder) detailed broad mechanisms of tongue protrusion in animal models (Hiiemae and Crompton, 1985; Smith, 1986, 1984), but were limited in spatial resolution and, due to the invasive nature of the method, could not be extended to humans. Electromyography (EMG) studies of the genioglossus with intraoral (Doble *et al*, 1985) or intramuscular (Krol *et al*, 1984; Sauerland *et al*, 1976) wire electrodes have yielded insight into gross myoelectric activity and physiologic muscle recruitment. However, intramuscular electrodes are invasive in nature and ambiguous in signal source. Intraoral (surface) electrodes are less invasive, but are limited to testing only surface

myoelectric activity, which introduces difficulty in deriving distinct fiber population activity in an organ with such a compact, interwoven muscular mesh.

Direct methods for non-invasive measurement of muscle deformation have been developed using various magnetic resonance imaging techniques, such as phase-contrast imaging, to derive strain rates (Drace and Pelc, 1994; Wedeen, 1992). Another MRI method is to apply rectilinear magnetic tags that deform with deforming tissue (SPAMM, or Spatial Modulation of Magnetization) (Axel and Dougherty, 1989; Azhari *et al*, 1993; Moulton *et al*, 1996; Niitsu *et al*, 1994; Young and Axel, 1992; Young *et al*, 1993; Zerhouni *et al*, 1988). The latter technique has been applied to study cardiac strain and contractility, but certain caveats do exist. While strain constitutes a measure of localized deformation, it is only a secondary marker of contraction or relaxation. For instance, contracting fiber bundles, such as fibers of the extrinsic palatoglossus or styloglossus, can deform adjacent regions in the tongue (and induce compressive strain) in the absence of direct muscular contractions in those regions. In the current study, the technique of tagged magnetization was extended to assess regional strain in the tongue during *in-vivo* physiological motion. The technique was further optimized by maximizing the number of tracked deforming elements and providing quantification of discrete element deformation with spatially resolved strain mapping. Three cardinal motions of the tongue were studied: protrusion out of the oral cavity, protrusion with lateral bending, and sagittal bending with tongue tip toward the hard palate. These motions can be considered foundations of the more complex physiological motions involved in deglutition and phonation.

Intramural strain during deglutition was also investigated. Abnormal swallowing is known as dysphagia, which is a symptom of underlying disease technically defined as an "abnormality in the transfer of a bolus from the mouth to the stomach" (Groher, 1997). The incidence of dysphagia has been reported as 35% in people aged 50-79 and 32% of all patients in intensive care units. The high incidence of this symptom provides the motivation for this and all subsequent research efforts. During normal swallowing, the tongue undergoes a stereotypical sequence of muscular deformations. The ingested bolus is initially contained in a groove-like depression in the middle dorsal surface of the tongue (early accommodation). This surface depression is then translated in a posterior

direction until the bolus comes to rest at the posterior edge of the tongue (late accommodation). Finally, the oral stage of the swallow is concluded by the rapid clearance of the bolus retrograde into the oropharynx at speeds approaching 100 cm/s (Miller A., 1982). The extent of muscular tissue deformation may vary under normal conditions as a function of bolus volume (Dantas *et al*, 1990) or viscosity (Pouderoux and Kahrilas, 1995), whether the bolus is solid, liquid, or even a sword (Devgan *et al*, 1978). Muscular deformation may also be modified by pathological effects on muscle contractility and/or neuromuscular regulation (Miller, 1982).

2 Deriving Myoarchitecture with Diffusion-Tensor MRI

The three-dimensional myoarchitecture of the mammalian tongue was derived by visualization of the diffusion tensor field. This technique was both non-invasive and capable of deriving fiber angle orientations, thus compiling a virtual anatomical atlas of the investigated muscle tissue.

2.1 Methodology

Magnetic resonance imaging was performed on 4 *ex-vivo* cow tongues obtained from Blood Farms (West Groton, MA). The excision was performed by first making an incision from the thyroid prominence to the angle of the mandible to expose the tongue, followed by an en bloc resection. Whole tongue specimens were refrigerated and scanned within 24 hours of harvest.

Diffusion tensor MRI was performed on fresh excised cow tongues; refrigerated and scanned within 24 hours of harvest. For each specimen, data were acquired for contiguous slices perpendicular to the antero-posterior axis of the tongue. Data were acquired at 1.5 T with 20cm receive-transmit head coil and a diffusion-sensitive stimulated echo pulse sequence. Stimulated echo sequences are preferable to their spin echo counterparts because they allow higher b-values to be realized with average magnetization gradients (Norris and Niendorf, 1995). Furthermore, they allow for longer diffusion times because the longitudinal magnetization, which is used for the stimulated echo, is being stored during the diffusion, or mixing time TM, and is not subject to transverse T_2 decay. Unfortunately, stimulated echo sequences have only half the signal to noise ratio (SNR) of spin echo techniques, necessitating considerable averaging. The sequence incorporated single-shot echo-planar spatial encoding with TE/TM/TR = 54/480/800 ms and spatial resolution of 3 x 3 x 6 mm. Using 16 signal averages, acquisitions were completed in 3 minutes per slice yielding an SNR of approximately 40:1 (glossal-to-background magnitude ratio) in the unattenuated images S_0 (diffusion sensitizing gradients off) and mean SNR of approximately 20:1 in the attenuated images S_k (diffusion sensitizing gradients on).

Diffusion sensitization utilized gradient pulses of amplitude |G| = 100 mT/m and duration δ = 10ms corresponding to net a spatial modulation $\|\mathbf{k}\| = 2\pi\gamma_H\delta|G| = 40$ radians/mm (γ_H is the proton gyromagnetic ratio, **k** is a column vector). Using an interpulse delay Δ = 500 ms, the diffusion sensitivity |b| factor was calculated to be

$$|\mathbf{b}| = \int_{\Delta} \mathbf{k}^T\mathbf{k}\, dt \approx |\mathbf{k}|^2 \Delta \approx 850\,\mathrm{mm}^2/\mathrm{sec} \qquad (7.0)$$

The magnetic field gradients were applied in 6 directions, corresponding to spatial modulations $\mathbf{k}_i$, i = 1...6. Thus, the applied magnetic field gradient vectors were as follows: $|\mathbf{G}_i| \approx \{\{\pm1,1,0\}^T, \{1,0,\pm1\}^T, \{0,\pm1,1\}^T\}$, and could be visualized as the non-opposing edge-centers of a cube, with its origin at the center. Hence, data acquisition for each slice consisted of seven images total: six images with gradients on, S_k, and one unattenuated image, S_0. Six gradient directions were necessary to completely span the 6 degree of freedom space of the diffusion tensor, which is a second order, symmetric, positive definite tensor. The diffusion tensor was computed at every voxel location by inversion of the linear matrix equation for diffusion attenuation. For the stimulated-echo pulse sequence

$$\log\left(\frac{S_k}{S_o}\right) = -\int_{\Delta} \mathbf{k}^T\mathbf{D}\mathbf{k}\, dt \approx -\Delta\mathbf{k}^T\mathbf{D}\mathbf{k} \qquad (8.0)$$

where S_k is the signal amplitude observed after spatial modulation **k,** and **D** is the diffusion tensor.

The diffusion tensor fields were displayed by color-coded 3D graphics. To depict fiber orientation, the diffusion tensor at each location was represented by an octahedron whose 3 axes were determined by the diffusion tensor eigensystem; octahedra axes were oriented in 3D space along the eigenvectors, $\mathbf{v}_i$, and scaled in length by the eigenvalues, λ_i. With a conventional ordering of the eigenvalues $\lambda_i > \lambda_j$ for i > j, the principal fiber orientation at each location was indicated by the leading eigenvector, $\mathbf{v}_1$. In addition, octahedra were color-coded using the standard assignment of vector-components to color-channels: $\{|v_{1x}|, |v_{1y}|, |v_{1z}|\} \in$ {red, green, blue} in order to improve the clarity of the images.

Furthermore, the distinct cross-fiber structure of the anterior tongue was represented by a different graphical technique in a single representative axial slice. This involved

visualizing the diffusion tensor at each voxel by a circular cylinder whose central axis was $\mathbf{v}_3$ and whose ends were parallel to the local $\mathbf{v}_1$-$\mathbf{v}_2$ plane. As discussed below, this plane was the direction in which the fiber orientations have greatest angular dispersion. Diffusion anisotropy in this slice was calculated by an index equal to the difference of the first two eigenvalues ($A_{ind} = \lambda_1 - \lambda_2$). Two, and not all three, eigenvalues were necessary to define an anisotropy index because the diffusion tensor field for a given tissue has the property of trace invariance (Pierpaoli and Basser, 1996), thus the third eigenvalue is a dependant quantity.

2.2 The Diffusion Tensor Map

The myoarchitecture of the tongue was analyzed by visualizing the diffusion tensor field (Figure 3). The data is presented as a sequence of coronal slices. The diffusion tensors corresponding to each voxel have been rendered as octahedra, and color-coded based on the principal eigenvector such that the antero-posterior fiber orientation is blue, medial-lateral fiber orientation is red, and inferior-superior fiber orientation is green. The posterior tongue demonstrated a central region of fibers originating at the inferior surface and projecting in a fan-like manner in the superior, lateral, and posterior directions (corresponding to the genioglossus). Lateral to this central region were two populations of fibers, the first directed posterior and inferior (corresponding to the hyoglossus) and the second directed posterior and superior (corresponding to the styloglossus). The anterior body of the tongue consisted of a central region of orthogonally oriented intrinsic fibers surrounded by a sheath-like tract of longitudinally-oriented fibers.

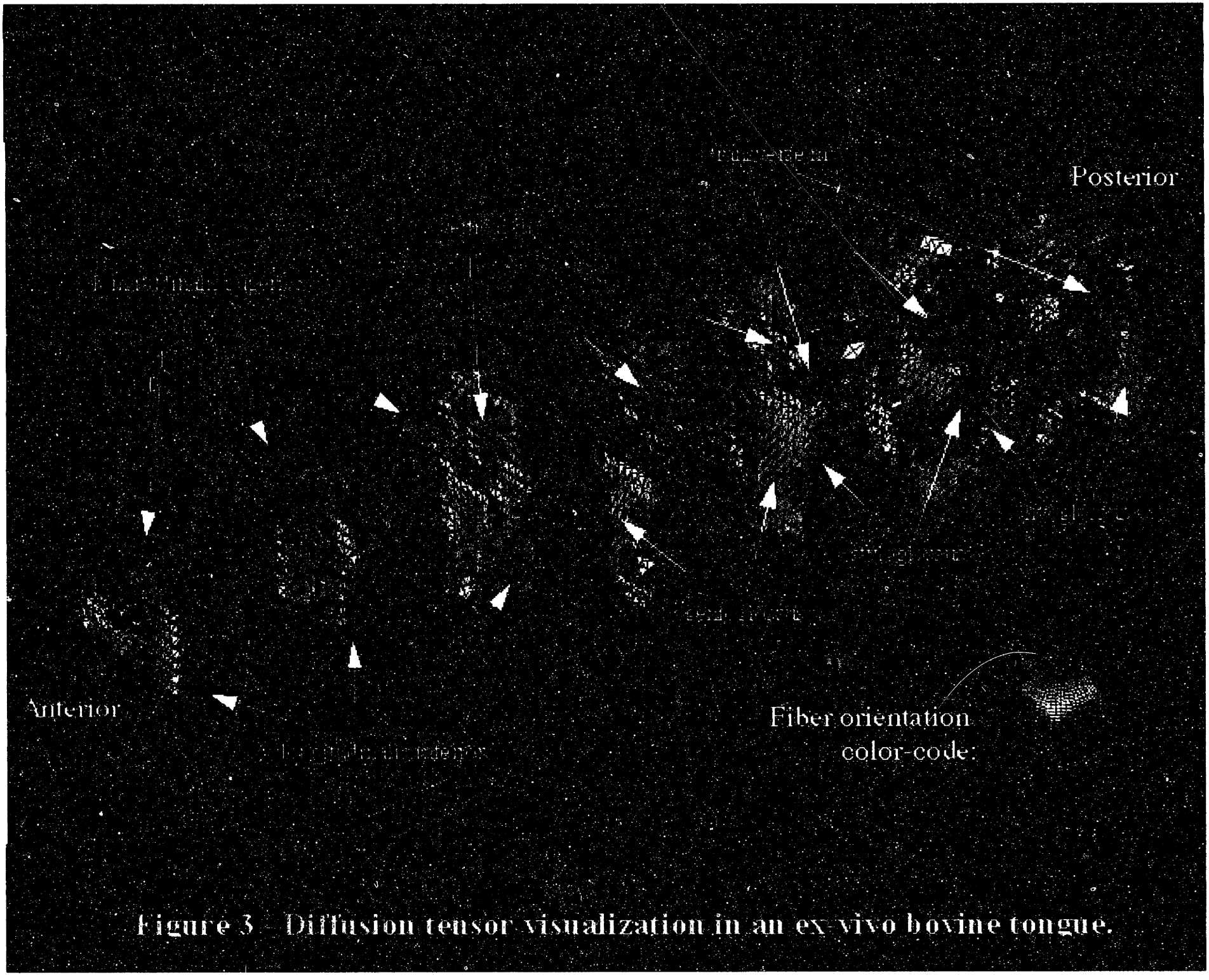

Figure 3 Diffusion tensor visualization in an ex vivo bovine tongue.

2.3 Angular Dispersion in the Anterior Tongue

Owing to the distinction in the anterior tongue between the orthogonal core fibers and the longitudinal sheath fibers, this tissue region was further analyzed by depicting graphically its two-dimensional architecture (Figure 4). In this data rendering, $\mathbf{v}_1$, $\mathbf{v}_2$ constitute the face of a flattened cylinder. These data are shown for the 3rd (anterior to posterior) slice of the complete diffusion tensor data set (Figure 3). This image depicts striking contrast between the core fibers, consisting of the vertical and transverse fibers, and sheath fibers formed by the longitudinalis muscles. This data also demonstrates a subtle bifurcation of the core into two large circular whorls, symmetrically placed about the sagittal midplane. More posterior slices show that these whorl patterns ultimately become confluent. The core is, thus, depicted architecturally as a forked structure, with the base of the structure in the posterior tongue and the two extensions in the anterior tongue. The fiber planes of the tongue sheath, by contrast, are concentric with the surface of the tongue, and locally parallel to the adjacent surface of the tissue.

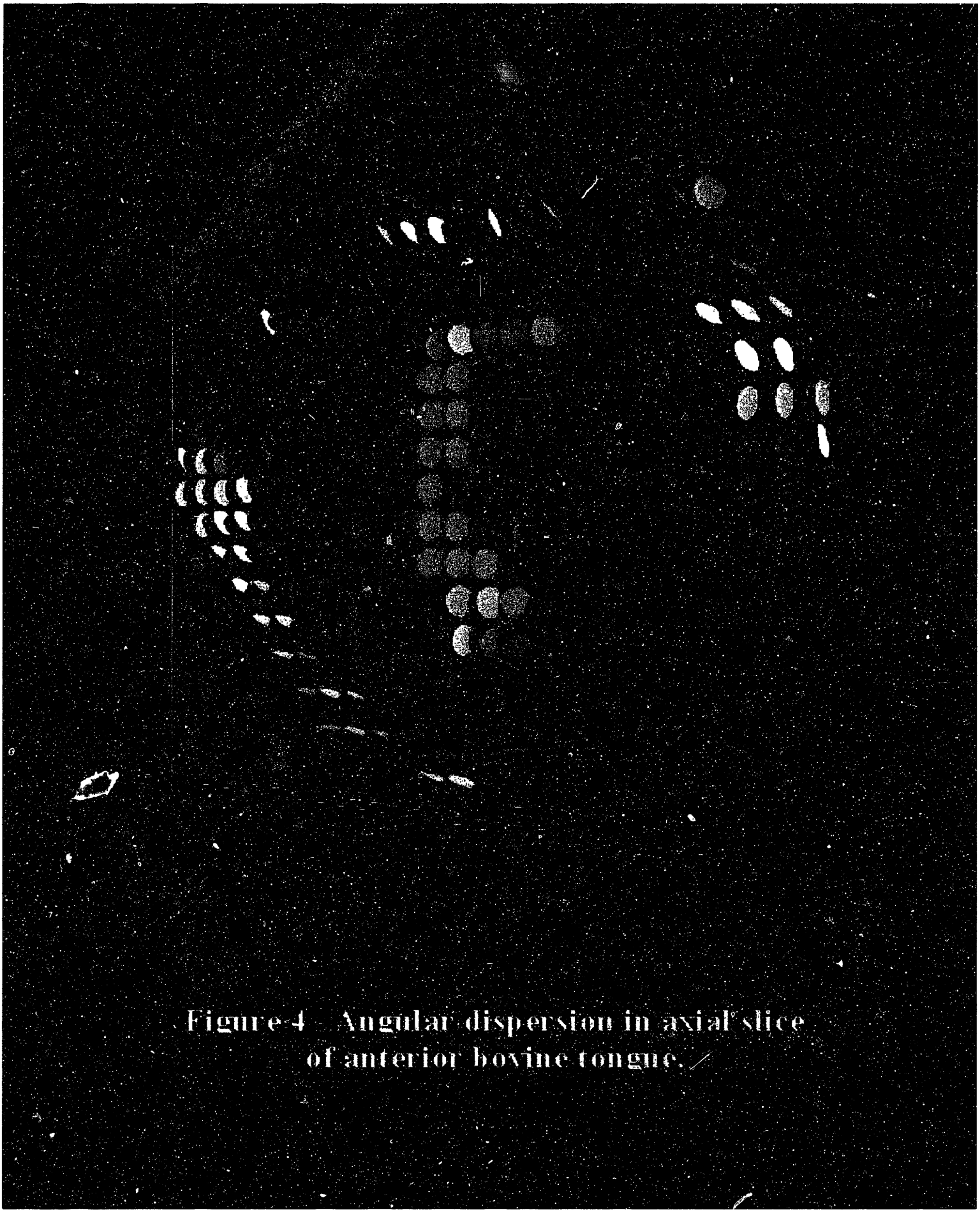

Figure 4 Angular dispersion in axial slice of anterior bovine tongue.

2.4 *Anisotropy*

Quantitative distinction between the core and sheath in the anterior tongue was provided by scalar measurement of diffusion anisotropy. Figure 5 shows a scatter plot of the diffusion anisotropy index, represented as $A_{ind} = \lambda_1 - \lambda_2$ vs. the fiber angle relative to the antero-posterior axis. These data were bimodal in that voxels whose principal eigenvector was parallel to the A-P axis, representing the longitudinal muscular sheath, had the highest diffusional anisotropy; whereas voxels whose principal eigenvector was perpendicular to the A-P axis (such as medial-lateral or inferior-superior: the core intrinsic muscles), showed lowest diffusional anisotropy.

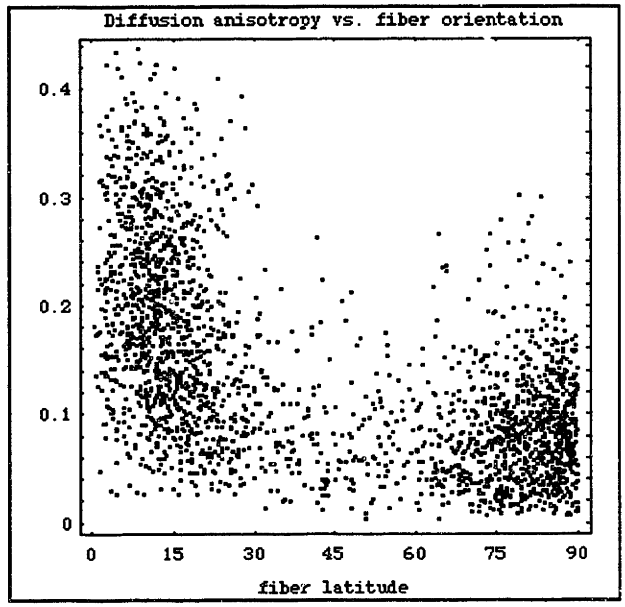

Figure 5 - Diffusion anisotropy, $\lambda_1 - \lambda_2$, as a function of fiber azimuth angle with respect to the antero-posterior axis of the tongue. Fibers of the tongue core (60-90° azimuth) have lower anisotropy than fibers of the sheath (0-30° azimuth).

3 Deriving Tissue Physiology with Tagging MRI

3.1 Tagging Methodology and Analysis

3.1.1 Magnetic Resonance Imaging

MR imaging was performed with a 1.5 Tesla Siemens Vision MRI system and an anterior neck coil using a single-shot fast asymmetric gradient echo pulse sequence. The imaging parameters were as follows: TR/TE 2.25/0.8 msec, matrix size 80 x 128, slice thickness 10 mm, and effective spatial resolution 1.33 x 1.33 mm. The imaging pulse sequence was preceded by 90° RF tagging pulses which served to saturate the longitudinal magnetization of the affected tissue (Figures 6,7).

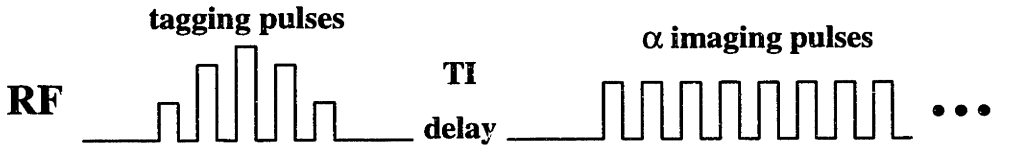

Figure 6a - Radiofrequency (RF) pulse sequence for setting up and imaging the MR tagging grid. The tissue deforms during the TI delay time.

The tagging pulses were arranged in a 1-4-6-4-1 power configuration to simulate a sinc shape. The summation of the entire tagging pulse train amounted to a 90° pulse; that is, it would flip the magnetization vector of the tagged tissue completely onto the transverse plane, thus saturating the effected magnetic spins. The Fourier transform of the comb function in a sinc envelope is an equally spaced, constant intensity banded grid. Hence, this sequence was applied in two orthogonal directions to comprise a square, rectilinear tagging grid (Figure 6b). The

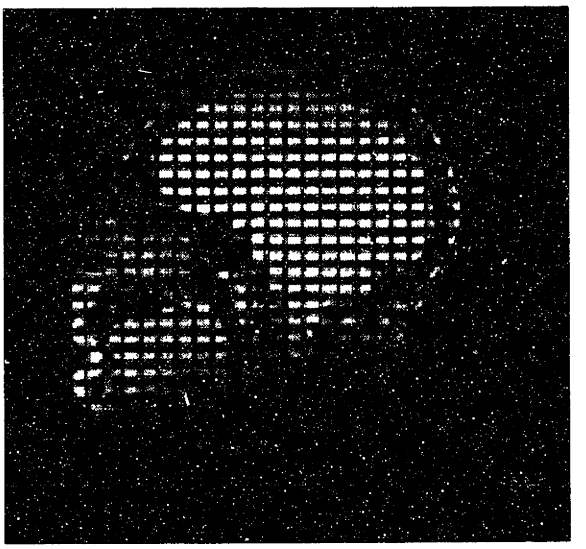

Figure 6b - tagged undeformed image

spacing of the tags on the image could be altered by altering the spacing of the tagging RF pulses, while the width of the tags could be altered by altering the width of the entire tagging RF pulse train. The imaging portion of the sequence (TurboFLASH), consisted of small flip angle (8°) alpha pulses which provided enough transverse magnetization to derive an asymmetric gradient echo. The entire imaging portion of the sequence lasted 180ms. K-space (frequency domain) was traversed asymmetrically (half Fourier space sampling) with 80 phase encode steps and 128 frequency encode samples. The image was then reconstructed with an inverse Fourier transform of the data from half of the frequency space. It is important to note that the entire sequence was "single-shot"; that is, no averaging, partial k-space reconstruction, or gating was necessary.

Since the relative brightness of a pixel (in a proton density weighted image) is due principally to the amount of longitudinal magnetization just prior to the imaging pulse sequence, tissue affected by the tagging pulses appeared dark in contrast to the surrounding tissue. The tagged tissue's longitudinal magnetization decays back to M_0 exponentially with rate constant T_1 (Figure 7). Thus T_1 limits TI, the length of delay time from tagging to imaging when the motion occurs, and also limits the maximum length of physiologic motion that can be studied (T_1 for tongue skeletal muscle was found to be 870ms, thus maximum TI was approximately 1100 ms).

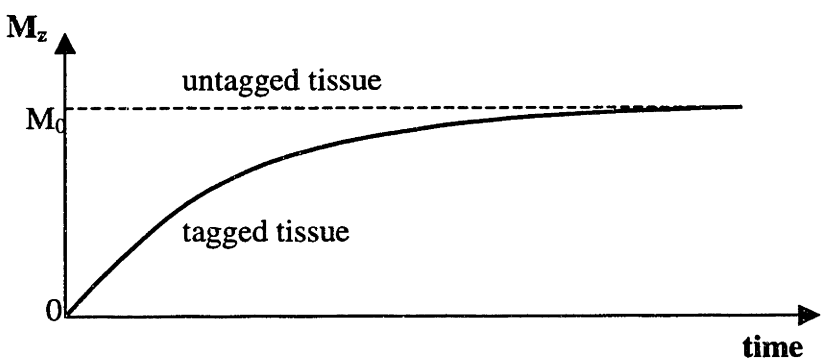

Figure 7 - The effect of RF tagging pulses on M_z, the longitudinal magnetization. The difference between the tagged and untagged tissue curves represents tag contrast.

3.1.2 Post Processing Data Analysis

3.1.2.1 Stain quantification of the deformed tagged image

Derivations for the following analysis methodology have been included in the appendix. Deformation can be quantified in image post-processing with measures of non-linear strain, a unitless measure of localized deformation. Inasmuch as relatively large strains were predicted for this tissue, the non-linear Green's strain tensor was used:

$$\mathbf{E}_{\text{Green}} = \frac{1}{2}\left(\mathbf{U}^2 - \mathbf{I}\right) \tag{9.0}$$

Where **U** is the right stretch tensor and **I** the identity tensor. The relationship between axial stretch and various strain definitions linear and non-linear (Green, Hencky-logarithmic) shows that while the three converge at stretch values close to unity (small strain approximation), there are significant differences when deformations are finite, necessitating non-linear strain measurements (Figure 8).

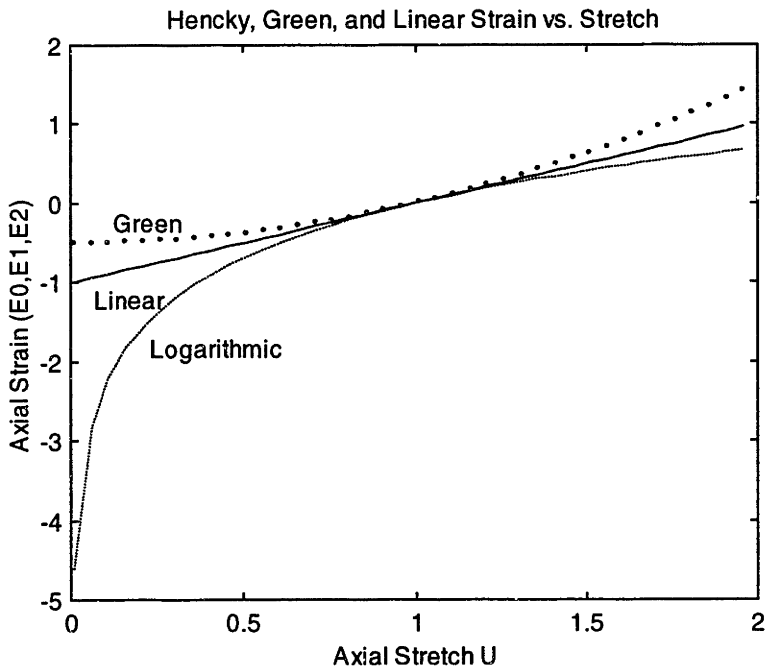

Figure 8 - Linear and non-linear axial strain vs. axial stretch

While the Green strain tensor is a valid non-linear measure of finite strain, it contains, by definition, an asymptotic limit for compressive strain of -0.5. This conclusion is derived from taking the limit of equation (1.0), as stretch approaches zero. Thus, the

positive limit (+∞) and the negative limit of the strain measure used are unequal, and any comparison of positive and negative strain results must consider this asymmetry. For example, under hypothetical axial strain conditions, a 50% compression of tissue stretch (a line segment of unit length contracting to a length of 0.5) would correspond to a strain of -0.375, whereas a 50% expansion of tissue stretch (a line segment of unit length expanding to a length of 1.5) would correspond to a strain of 0.625.

In order to resolve the idealized material continuum of the tongue, discrete triangular deforming elements were defined by digitizing nodes at tag line intersections. Thus each triangular element was composed of two independently deforming line elements; one along the x-axis and the other along the y-axis in the rest configuration. Each line element had length s at rest defined by the tag spacing. Axial strains were calculated based on the lengths of the deformed line elements (s_1 and s_2 respectively), while shear strain was calculated based on line element lengths, as well as the relative angle between adjacent line elements (90° - ϕ):

$$E_{xx} = \frac{1}{2}\left(\frac{s_1^2}{s^2} - 1\right) \tag{10.1}$$

$$E_{yy} = \frac{1}{2}\left(\frac{s_2^2}{s^2} - 1\right) \tag{10.2}$$

$$E_{xy} = \frac{s_1 s_2}{2s^2}\sin\phi \tag{10.3}$$

Although this tagging technique is inherently two-dimensional, the out-of-plane axial strain was calculated knowing the 2-D strain condition, assuming that tongue muscle is incompressible (hence isochoric), and out-of-plane shear strains are negligible:

$$E_{33} = \frac{1}{2}\left(\frac{1}{(1+2E_{11})(1+2E_{22})} - 1\right) \tag{11.0}$$

where E_{11}, E_{22}, and E_{33} are the principal strains. Since E_{xz} and E_{yz} are assumed nil, $E_{zz} = E_{33}$ regardless of the reference frame, and thus, each finite triangular element in the tagging grid has an associated non-linear (Green's) symmetric strain tensor given by

$$\begin{bmatrix} E_{xx} & E_{xy} & 0 \\ E_{yx} & E_{yy} & 0 \\ 0 & 0 & E_{zz} \end{bmatrix} \tag{12.0}$$

Directional axial or shear strains were represented individually as a color-coded "map" overlaying the original tagged image. This map constituted a pseudo-surface whose height at a given spatial location was defined by the amount of strain at that location, as determined by its proximity to a finite element centroid. The surface was smoothed by bi-cubic approximating splines.

The entire strain tensor was alternately represented by a spatial array of octahedra, with each octahedron centered on a tagging element's centroid. The major and minor axes of these octahedra were oriented according to the directions of the eigenvectors, and scaled to the linear directional axial stretch measured in the given tagging element. In addition, the relative size of an octahedron was based on a scaling factor, f, defined by a function of the strain tensor's independent eigenvalues (λ_1, λ_2):

$$f = \sqrt{\lambda_1^2 + \lambda_2^2} \tag{13.0}$$

3.1.2.2 Statistical analysis

In order to study tongue bending a plot of tissue strain versus distance from the inside edge of the bend was created. The relationship between these two variables was explored with the linear correlation coefficient. A single row of elements along the transverse section at maximum curvature was studied in each tongue. The variables were normalized such that the strain measure was divided by the maximum strain in the given row, and the distance from inside edge was divided by the width of the tongue along the radius of maximum curvature. This normalization allowed for the comparison of data points from tongues of various shapes and sizes, undergoing various degrees of bending.

Inter-subject variation during swallowing was accounted for by a statistical treatment of the strain data. In order to obtain mean directional strain data, four regions in the mid-sagittal slice of the tongue (anterior, mid-superior, posterior, and inferior - Figure 9) were sampled in the x, y, and z directions. Data were analyzed for each region for three phases of oral stage deglutition: early accommodation, late accommodation, and propulsion. P-values were computed for a one-sided t-test, which tested whether or not a sample mean

was significantly greater than or less than zero. The means and standard errors for the one-sided t-test were computed for each condition.

Based on previous determinations of tissue myoarchitecture and function in the mid-sagittal plane, the anterior tongue region (region 1) encompasses the tongue's intrinsic musculature (transversus, verticalis, and longitudinalis muscles). The middle superior tongue region (region 2) encompasses the anterior fibers of the genioglossus muscle and a portion of the intrinsic muscles. The posterior tongue region (region 3) encompasses predominantly the posterior fibers of the genioglossus muscle. While regions 2 and 3 subdivide the genioglossus muscle, there is precedent for heterogeneous, localized activity in this muscle, as has been previously suggested by EMG studies (Miyawaki *et al*, 1976). The inferior tongue region (region 4) encompasses the inferior fibers of the genioglossus muscle, as well as the geniohyoid muscle. The coordinate axes x, y, and z correspond to anterior-posterior (x-direction), inferior-superior (y-direction), and medial-lateral (z-direction) directions.

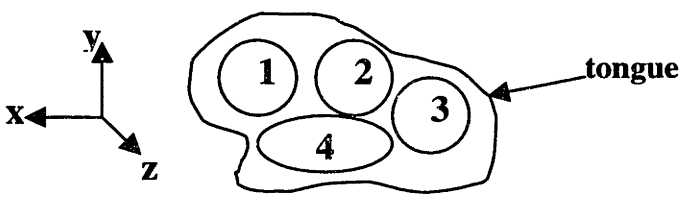

Figure 9 - Regional analysis of tongue mechanics
Segmentation of the mid-sagittal imaging slice into four functional regions. Region 1: intrinsic musculature, including transversus, verticalis, and longitudinalis. Region 2: anterior genioglossus and posterior intrinsic fibers. Region 3: posterior fibers of the genioglossus muscle. Region 4: inferior genioglossus and geniohyoid fibers. The coordinate axes x, y, and z correspond to anterior-posterior (x-direction), inferior-superior (y-direction), and medial-lateral (z-direction) directions.

3.2 Anterior Tongue Protrusion and Sagittal Bending

3.2.1 Protocol

Subjects (n = 6) were chosen for study who possessed no history or current abnormalities of speech or swallowing. These studies were approved by the Investigational Review Board of Beth Israel Deaconess Medical Center. For a given experiment, the protocol was as follows:

- application of magnetic tags to the resting undeformed tongue muscle tissue, which, through an audible click, prompted the subject to perform the prescribed tongue motion - anterior protrusion, sagittal or lateral tongue bending.
- time delay, TI (400 – 500 msec); during this time the tissue was deformed by voluntary action.
- imaging of the tagged, deformed tissue, held static in the deformed state by the subject; total imaging time was 180ms.

3.2.2 Results

The cardinal tongue motions of anterior protrusion (Figure 10), sagittal bending to the hard palate (Figure 11) and lateral tongue left (Figure 13) occurred as the result of coordinated intrinsic muscle contraction. The mechanical consequence of these contractions was depicted as strain tensors for individual elements, and represented as composite strain maps for each motion. Each strain map represented a single component of the strain tensor whose magnitude corresponded to a color-code and was referenced to resting tongue tissue. Negative strain values of -0.5 to 0 were represented as cyan and blue, while positive strain values of 0 to 2.0 were represented as green, yellow, and red.

Anterior protrusion produced positive strain in the anterior portion of the tongue, as evidenced by the strain tensor visualization (Figure 10c). The positive strain was along the axis of elongation (anterior-posterior, E_{xx}) and peaked at 2.184. This elongation coexisted with bi-directional contraction (negative strain) in the anterior tongue along the superior-inferior (E_{yy}) and medial-lateral (E_{zz}) axes. The contractile strain for the

displayed image was calculated to be as low as -0.381 and -0.458 in the y and z directions respectively. The lower portion of the tongue was strain free.

Sagittal tongue curl to hard palate produced positive anterior-posterior (E_{xx}) strain that peaked at 1.087 and increased with distance outward from the center of curvature (Figure 14, $r = 0.9216$, $p < 0.0005$). This graded extension was also seen in the strain tensor visualization (Figure 11c). For the displayed image, the elongation was due to a commensurately graded medial-lateral (E_{zz}) contraction that was as low as -0.447. Superior-inferior (E_{yy}) strain was mainly positive, peaking at 0.416. The lower portion of the tongue was strain free.

Lateral tongue curl left was fundamentally similar to sagittal tongue curl. Anterior-posterior (E_{yy}) strain was predominantly positive, peaked at 0.990 and increased with distance outward from the center of curvature (Figure 15, $r = 0.8978$, $p < 0.0005$). This graded extension was also evidenced by the strain tensor visualization (Figure 13c). For the image displayed, the elongation coexisted with a contraction in the superior-inferior (E_{zz}) direction whose lower bound was -0.353 and which decreased with distance from the center of curvature. The posterior of the tongue was under positive medial-lateral (E_{xx}) strain peaking at 0.827.

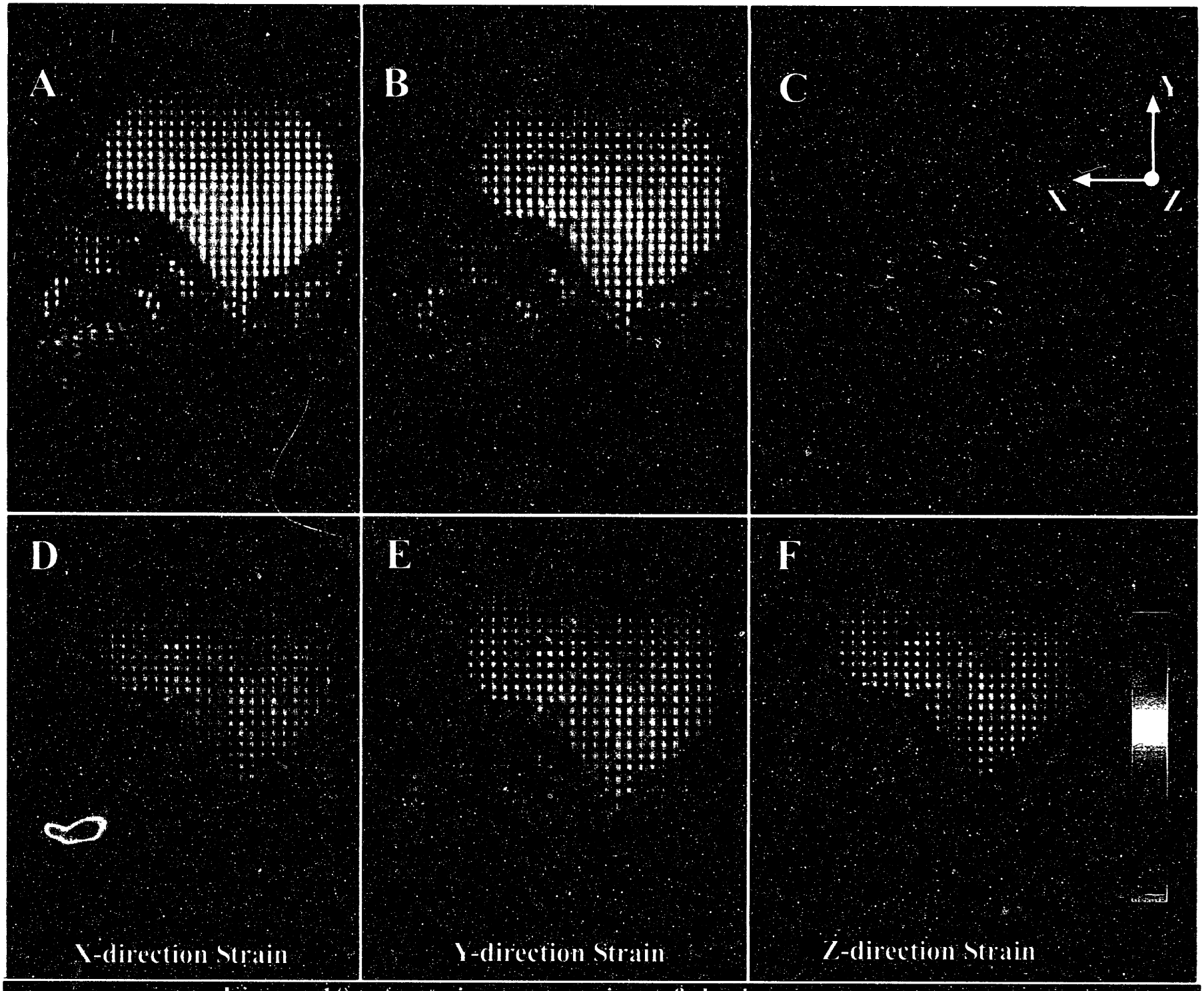

Figure 10 - Anterior protrusion of the human tongue.

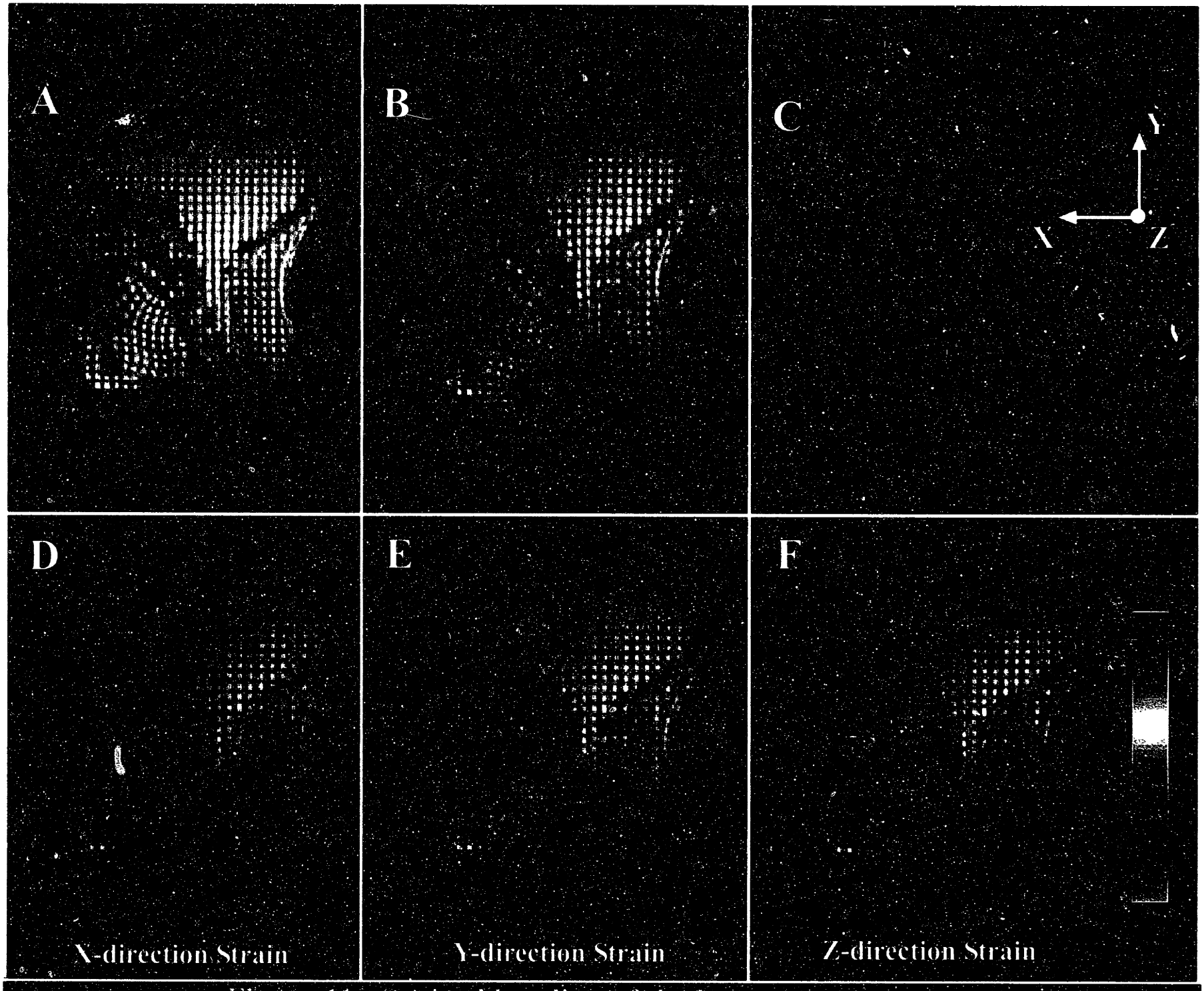

Figure 11 - Sagittal bending of the human tongue.

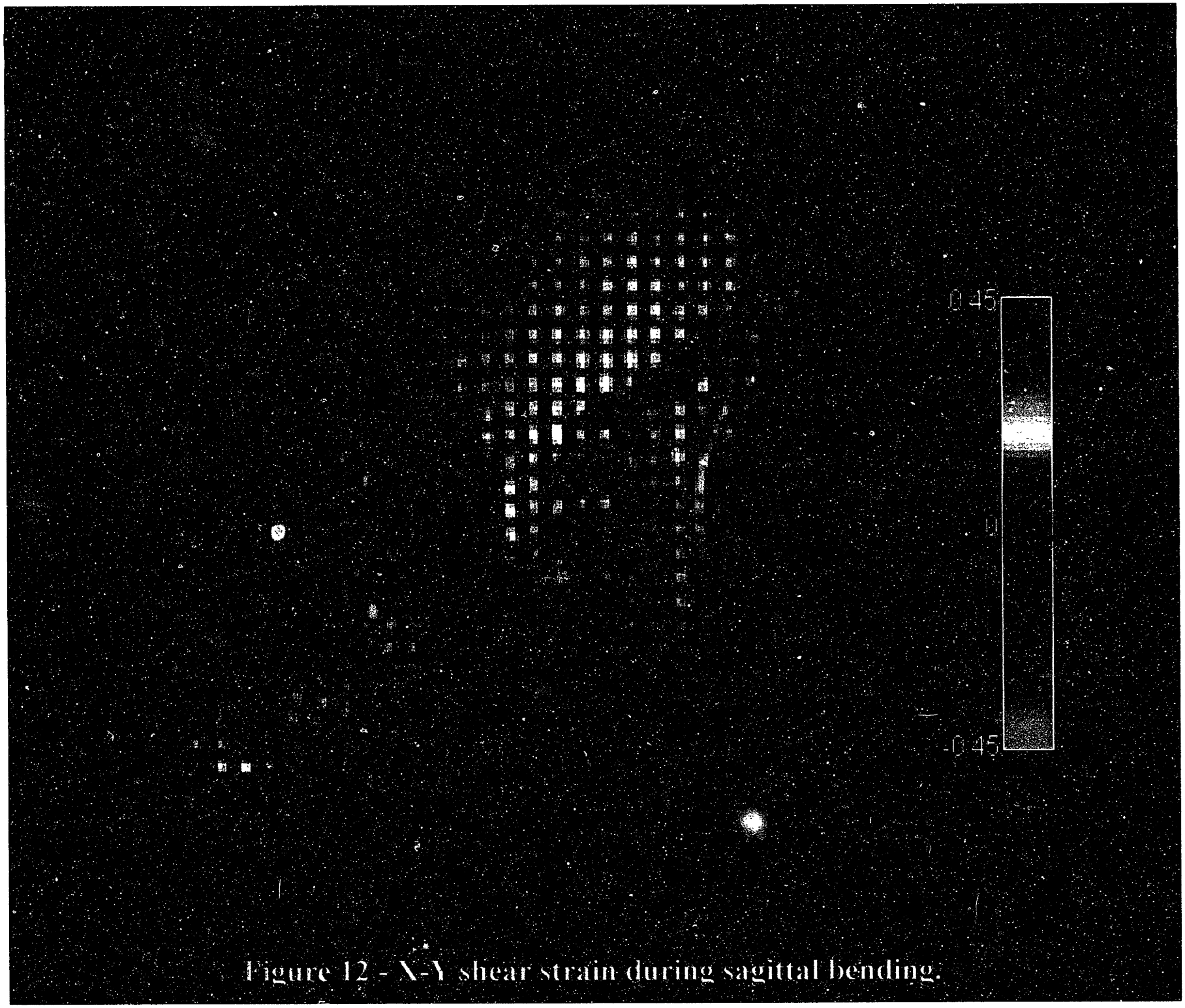

Figure 12 - X-Y shear strain during sagittal bending.

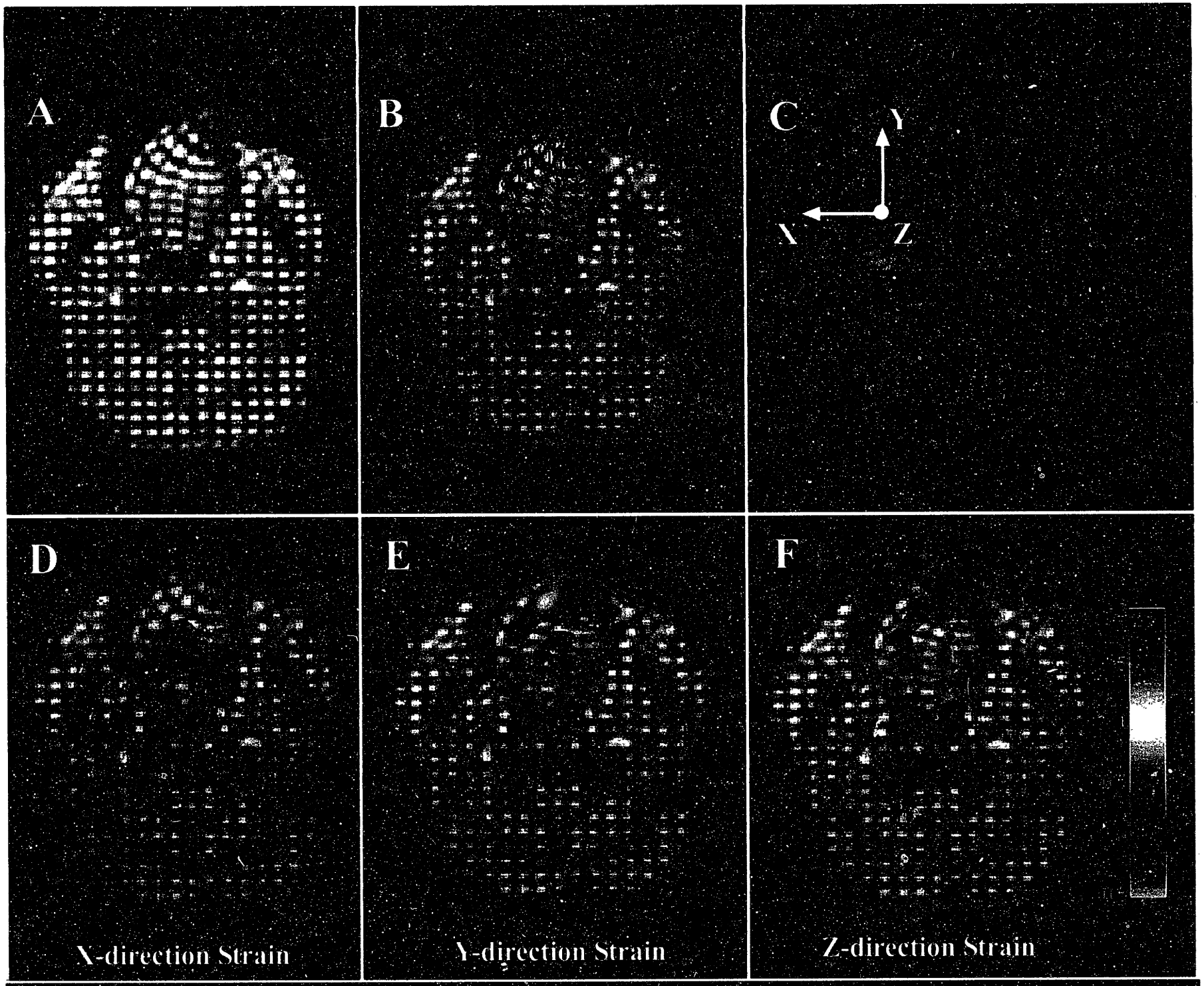

Figure 13 - Lateral bending of the human tongue.

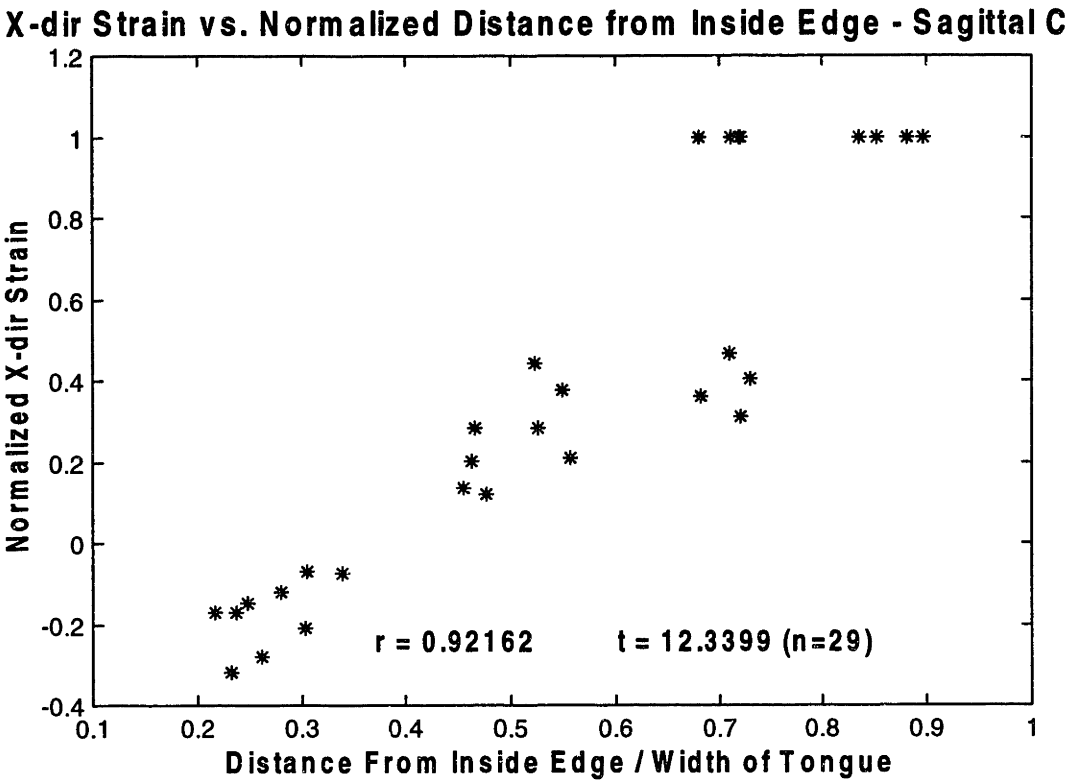

Figures 14 - Sagittal bending: x-dir axial strain vs. distance from inside edge of bend

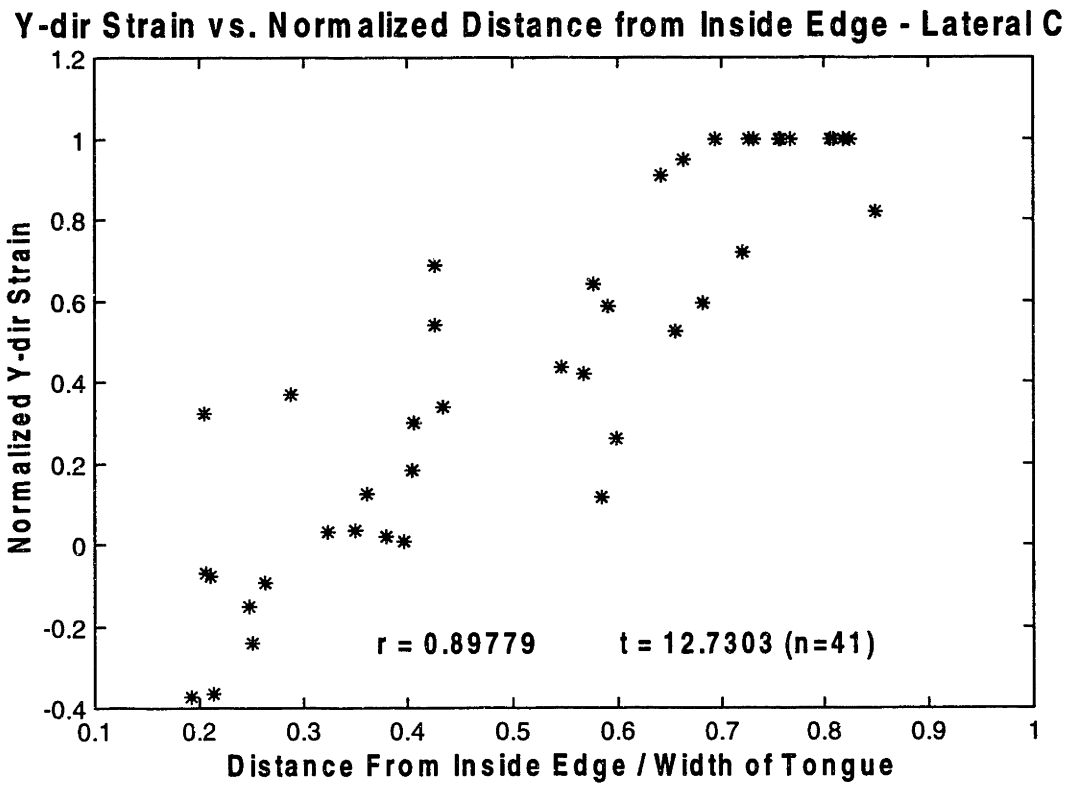

Figures 15 - Lateral bending: y-dir axial strain vs. distance from inside edge of bend

3.3 *Deglutition (swallowing)*

3.3.1 *Protocol*

Subjects (n = 8) were chosen for study who possessed no history or current abnormalities of speech or swallowing. These studies were approved by the Institutional Review Board for Human Research of Beth Israel Deaconess Medical Center. Dry (saliva only) swallows were elicited from the subjects, and magnetic resonance imaging was performed for each swallow. The timing of image acquisition was determined in order to visualize the various phases of oral stage deglutition.

For a given subject, the experimental protocol was as follows:

- application of magnetic tags to the resting undeformed tongue muscle tissue, which through an audible click, prompted the subject to swallow
- imposition of a variable delay time interval (300 – 800 msec, incremented by 100msec) to cover the different phases of the swallow (oral stage)
- imaging of the tagged, deformed tissue.

3.3.2 *Results*

Direction-dependent strain fields were acquired for the mid-sagittal slice of the tongue using a tissue tagging nuclear magnetic resonance technique. Normal subjects were studied during three phases of dry swallows: early accommodation, late accommodation, and propulsion. Strain data were visualized either as two-dimensional strain maps (axial strain in the x, y, and z directions) for representative subjects, or as octahedra representing the complete strain tensor (directional strain in principal directions) for each deforming element (Figures 16-18). In addition, inter-subject axial strain means for each of four functional regions of the tongue were also displayed (Table 1).

In early accommodation, the subject contained the bolus in the middle portion of the tongue's dorsal surface (Figure 16). The anterior tongue showed a characteristic pattern of positive (expansive) x-direction strain (peak strain 0.521), while the middle tongue showed negative (contractile) y-direction strain (peak strain -0.319), along with positive x

and z direction strain (peak strain 0.477 and 0.803, respectively). The posterior and inferior regions of the tongue demonstrated x direction expansion (peaking at 0.208 and 0.477, respectively). Inter-subject mean data corroborated these deformation patterns ($p<0.01$) (Table 1).

During late accommodation (Figure 17), with the subject holding the bolus in a posterior depression, the anterior tongue displayed positive y-direction strain (peak strain 0.151). The posterior tongue displayed significant negative y-direction strain (peak strain –0.302) with commensurate expansion along the x and z direction (peaking at 0.358 and 1.845 respectively). Inter-subject mean data also corroborated these deformation patterns ($p<0.01$) (Table 1). Thus, bolus accommodation (early and late) principally represents a combination of contraction of the intrinsic core muscles in the anterior tongue (with commensurate anterior or superior expansion), and inferiorly-directed contraction of the extrinsic muscles (genioglossus and hyoglossus) in the middle and posterior regions of the tongue.

During the propulsive phase of the swallow (Figure 18), the bolus is propelled retrograde into the oropharynx by posterior displacement and deformation of tongue tissue. During this phase, the strain results in the posterior genioglossus presented expansive x and y direction strain (peaking at 0.469 and 0.684 respectively), and contractile z direction strain (peaking at -0.374). These results were also seen as statistically significant deformation patterns in inter-subject mean strain calculations ($p<0.001$) (Table 1). This result was consistent with the existence of postero-superior directed passive stretch in the midline, and suggests concurrent contraction of the laterally inserted styloglossus (not visualized in the current study), as well as contraction of the z directed muscle fibers characteristic of the intrinsic transversus muscle.

	EARLY				LATE				PROP		
	zone 1				zone 1				zone 1		
direction	mean	st.dev	p-value	direction	mean	st.dev	p-value	direction	mean	st.dev	p-value
x	0.135	0.121	0.0081	x	0.027	0.063	0.1726	x	0.034	0.053	0.0680
y	-0.006	0.105	0.4345	y	0.136	0.089	0.0067	y	0.083	0.067	0.0085
z	0.034	0.114	0.2140	z	-0.048	0.066	0.0685	z	-0.031	0.064	0.1252
	zone 2				zone 2				zone 2		
direction	mean	st.dev	p-value	direction	mean	st.dev	p-value	direction	mean	st.dev	p-value
x	0.188	0.071	0.0001	x	-0.009	0.040	0.2981	x	0.065	0.081	0.0388
y	-0.165	0.054	0.00003	y	-0.074	0.062	0.0163	y	0.050	0.093	0.1045
z	0.179	0.114	0.0015	z	0.192	0.093	0.0020	z	-0.014	0.080	0.3323
	zone 3				zone 3				zone 3		
direction	mean	st.dev	p-value	direction	mean	st.dev	p-value	direction	mean	st.dev	p-value
x	0.083	0.057	0.0023	x	0.131	0.043	0.0003	x	0.173	0.045	0.00003
y	-0.034	0.035	0.0140	y	-0.125	0.061	0.0020	y	0.098	0.050	0.0010
z	0.021	0.054	0.1526	z	0.202	0.134	0.0071	z	-0.109	0.040	0.0002
	zone 4				zone 4				zone 4		
direction	mean	st.dev	p-value	direction	mean	st.dev	p-value	direction	mean	st.dev	p-value
x	0.093	0.046	0.0004	x	0.073	0.047	0.0063	x	0.064	0.044	0.0043
y	-0.050	0.063	0.0312	y	-0.010	0.070	0.3688	y	0.008	0.058	0.3713
z	0.032	0.072	0.1272	z	0.023	0.101	0.2984	z	-0.004	0.061	0.4275
n =	8			n =	6			n =	7		

Table 1 - Axial strain in the tongue during the functional phases of swallowing
Mean and standard deviation of axial strain in association with early accommodation, (n = 8), late accommodation (n = 6), and propulsion (n = 7), for each region of the tongue. The data is represented as axial strain along each spatial direction (x, y, and z).

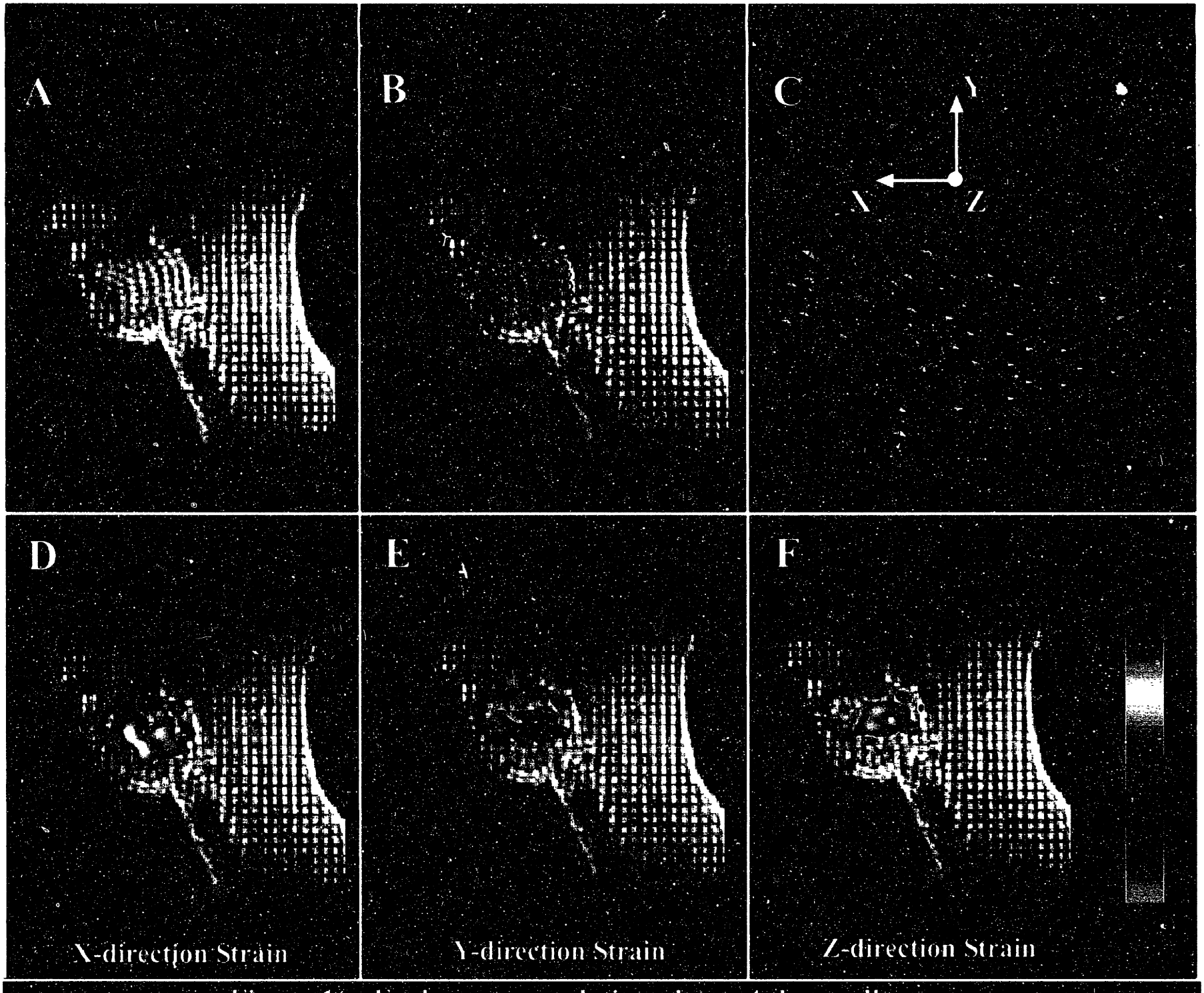

Figure 16 - Early accommodation phase of the swallow.

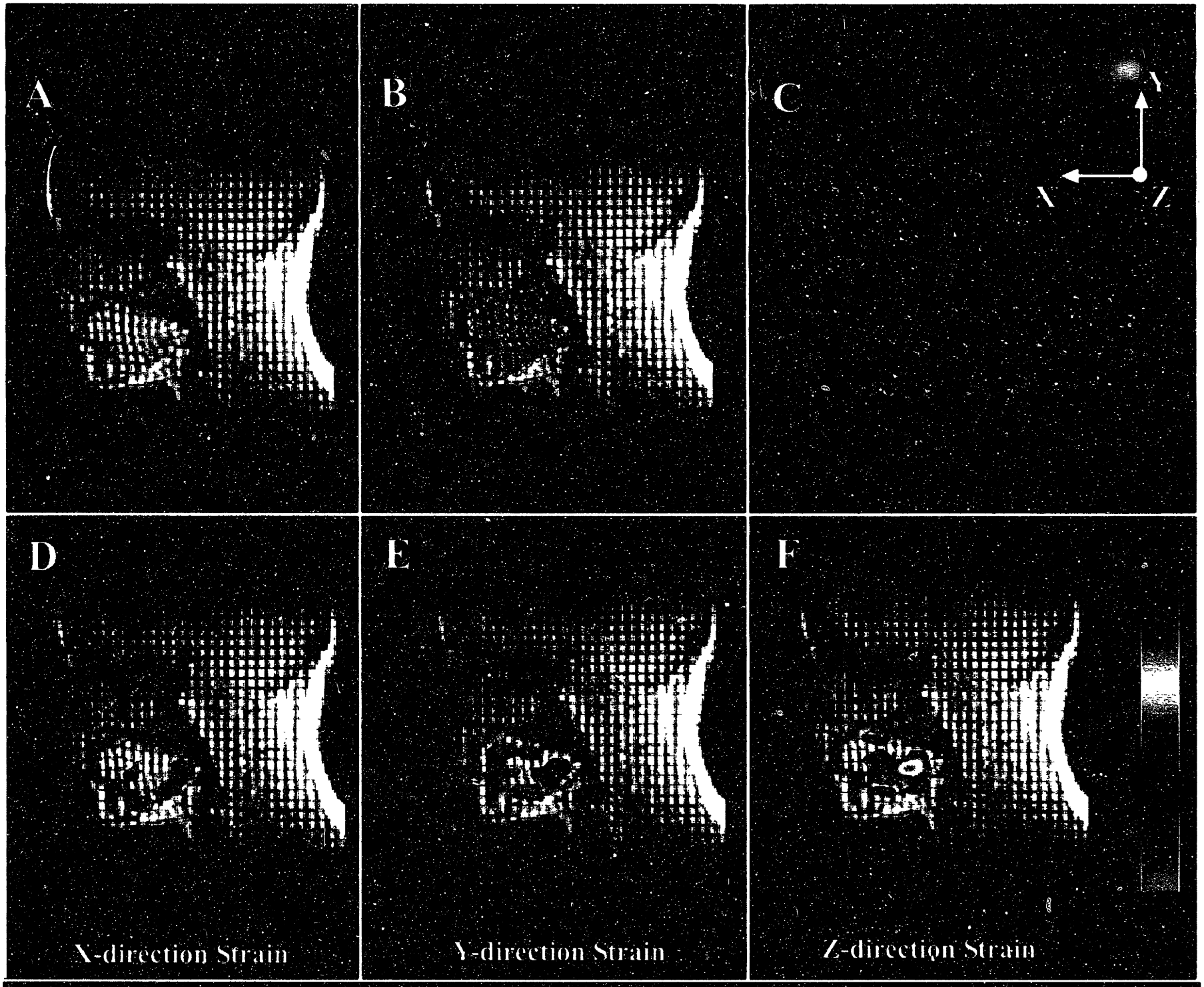

Figure 17 - Late accommodation phase of the swallow.

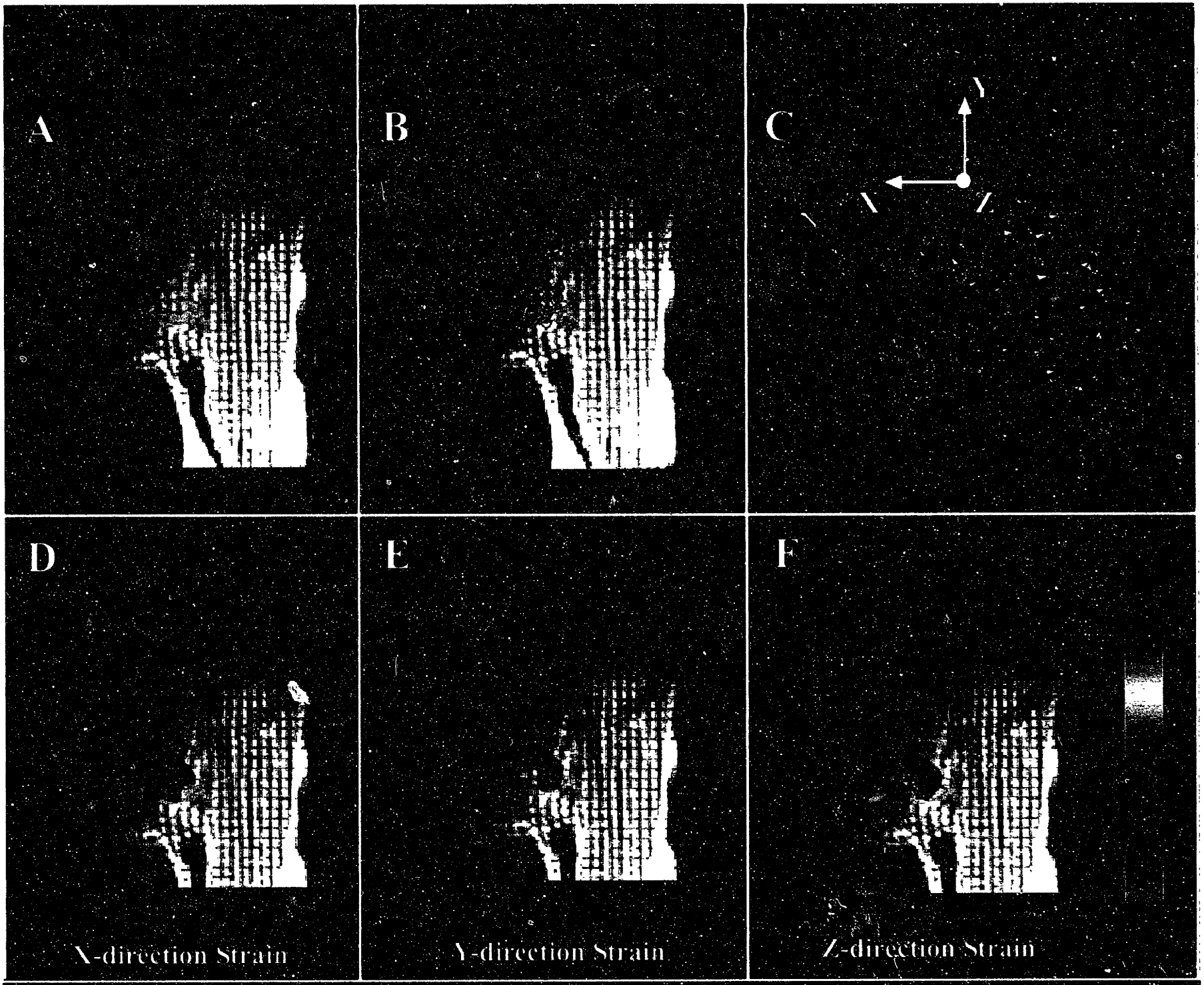

Figure 18 - Propulsion phase of the swallow.

3.4 *Error Analysis and Sensitivity Study*

Certain assumptions were made in the development of the previously described tagging MRI strain model. This section is an attempt to quantify the errors incurred by hypothetically erroneous assumptions, as well as to test the sensitivity of the model to these errors. There is also an attempt to quantify the errors introduced during data reduction, through manual image digitization.

3.4.1 Digitization Error

Manual digitization in tagging MRI post-processing analysis was subject to human error, as the operator, whether trained or not, must manually click on the perceived tag line intersection points. Digitization was done on a Dell 17" monitor with a resolution of 1280 x 1024 (width x height) in screen pixels. At maximum window size, the image (256x256) filled approximately 70% of screen height, thus the screen was composed of 366 image pixels, or 1 screen pixel = 0.357 image pixels.

In this analysis it will be assumed that the human digitization error was ±2 screen pixels and that the initial (undeformed) tag spacing was 5.1 image pixels. Because the strain calculation was non-linear, the error in axial strain will depend on the deformed tag spacing, s_1. Thus, the theoretical axial strain error can be expressed as the following difference:

$$\text{axial strain error} = 0.5*((s_1 \pm \epsilon)^2 / 5.1^2 - 1) - 0.5*(s_1^2 / 5.1^2 - 1) \qquad (14.0)$$

where $\epsilon = 0.714$ image pixels and $s_1 = 3$ to 10 image pixels (physiological range). The axial strain error has been plotted below, and shows a maximal error of 28.63% at a real strain of 142.2%. However, these errors would be most pernicious at small measured strains where they would comprise a higher percentage of the reported value.

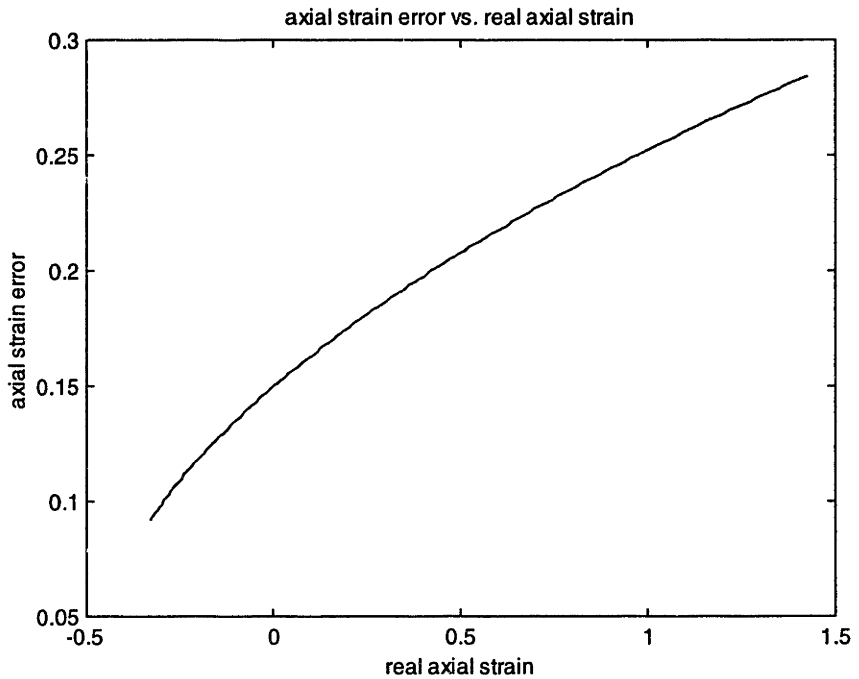

Figure 19 - Digitization strain error as a function the real axial strain

3.4.2 Incompressibility

In order to deduce the through-plane axial strain, E_{zz}, from data measured solely in the x-y plane, the model assumes incompressibility of the deforming muscle tissue. This constraint leads to the condition of isochoric or volume preserving deformation. Mathematically, isochoric deformation can be represented by setting the determinant of the deformation gradient, F, equal to unity. This leads to an expression for the unknown through-plane axial strain E_{zz} , which is equivalent to E_{33} (see appendix):

$$E_{33} = \frac{1}{2}\left(\frac{1+\epsilon}{(1+2E_{11})(1+2E_{22})} - 1\right) \tag{15.0}$$

where ϵ can range from -0.1 to 0.1 for reasonable physiological limits of tissue compressibility. Muscle tissue has been shown to be isochoric (maintaining its volume under deformation) or incompressible by x-ray diffraction methods (Elliot *et al*, 1963), thus a compressibility of 10% can be deemed conservative. The x-y plane principal strains, E_{11} and E_{22}, have been taken from an element in tongue protrusion which presented extreme values of strain: E_{11} = 2.123 and E_{22} = 0.232. The resulting percent

error compared to an E_{zz} calculated by assuming perfect incompressibility (E_{zz} = -0.435) has been plotted below. The maximum percent error was found to be only 1.5% at a value of 10% compressibility (deviation of 0.1 from a unity determinant).

Figure 20 - Percent error in calculating E_{zz} as a function of compressibility

3.4.3 Through Plane Shear Strains

An important assumption made in determining the through plane axial strain, E_{zz}, from the incompressibility condition was that through-plane shear strains, E_{xz} and E_{yz}, were negligible. This assumption was deemed reasonable by the fact that the motions studied were symmetric about the mid-sagittal plane. In order to test the sensitivity of the model to through-plane shears, representative elements were chosen from a tongue protrusion dataset (Table 1). This tongue motion was chosen since it involved extreme strain values; hence, element 39 was chosen for its extreme axial strain value, while element 30 was chosen for its extreme shear strain value. These elements were augmented as 39' and 30' to investigate the effect of variable in-plane axial and shear strain.

Element	E_{xx}	E_{yy}	E_{xy}
39	2.115	0.240	-0.125
39'	1.057	0.240	-0.125
30	0.737	0.604	-0.630
30'	0.737	0.604	-0.315

Table 2 - Elements used in sensitivity study (39: extreme axial strain; 30: extreme shear strain; 39', 30': augmented elements)

Elements 39 and 39' have similar E_{yy} and E_{xy} values, but element 39' was under half the axial strain, E_{xx}, as element 39. Elements 30 and 30' had similar axial strain values, but element 30' was under half the shear strain, E_{xy}, as element 30.

In order to derive the through plane axial strain, E_{zz}, the isochoric condition must be solved in terms of the known in-plane axial and shear strains, and through-plane shear strains.

$$E_{zz} = \frac{1}{2}\left(\frac{1-2E_{yz}\left(4E_{xy}E_{xz} - 2(2E_{xx}+1)E_{yz}\right) - 2E_{xz}\left(4E_{xy}E_{yz} - 2(2E_{yy}+1)E_{xz}\right)}{(1+2E_{xx})(1+2E_{yy}) - 2E_{xy}^2} - 1 \right) \quad (16.0)$$

The in-plane strains were taken from representative extreme strain elements, while through-plane shear strains, E_{xz} and E_{yz}, were identically incremented from a value of 0.0 to 0.7. The percent error in the new E_{zz} was computed relative to the E_{zz} value under zero through-plane shear strains.

The results of this study show several important findings (Figure 21). Firstly, through-plane shears always lead to a smaller calculated E_{zz}, i.e. negative percent error. Furthermore, through-plane shear strain greater than 20 or 30% can lead to significant errors in calculating E_{zz}, reaffirming the necessity that the motions studied be relatively symmetric about the x-y plane, minimizing through plane shear. Finally, the error was more sensitive to extreme E_{xy} values (element 30) compared to E_{xx} values (elements 39, 39'). This effect was also seen when comparing element 30 to 30'.

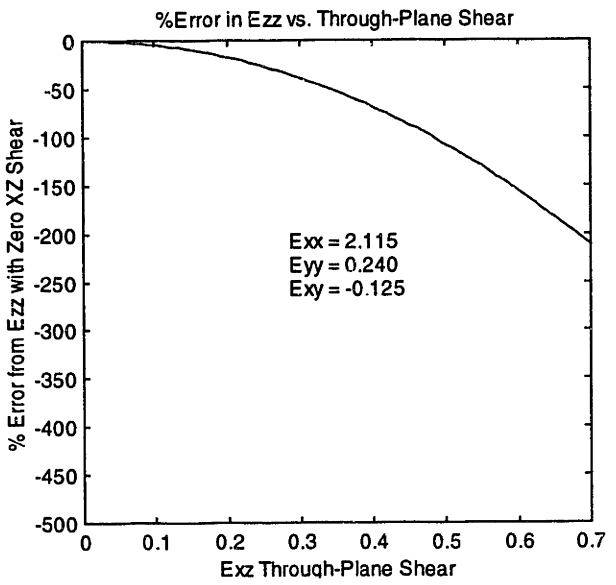

Element 39

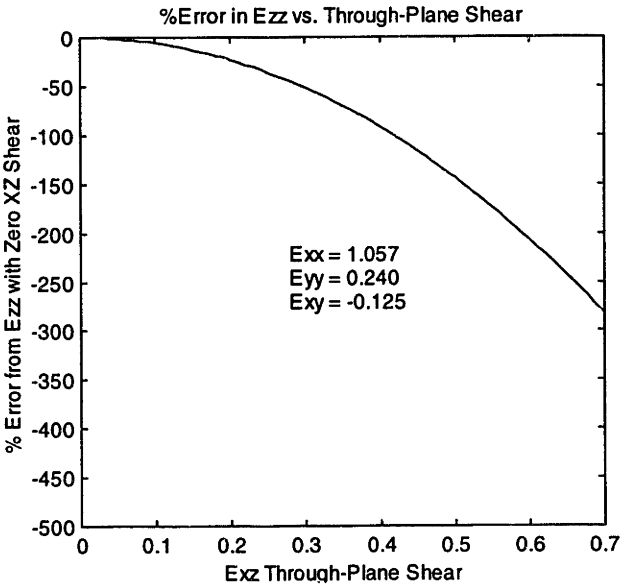

Element 39'

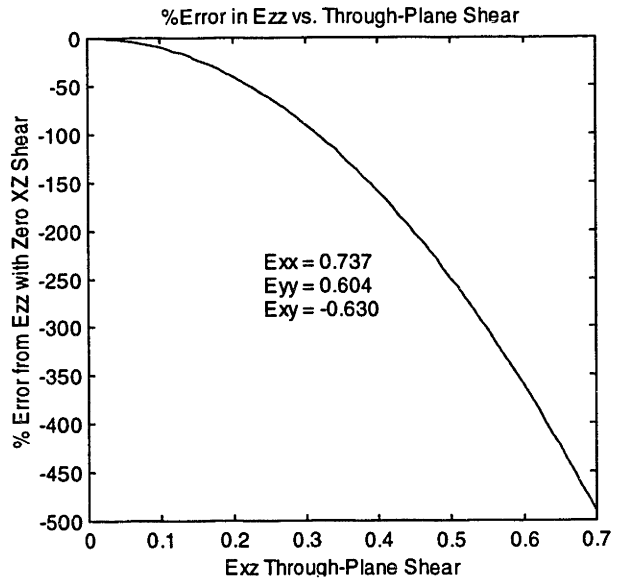

Element 30

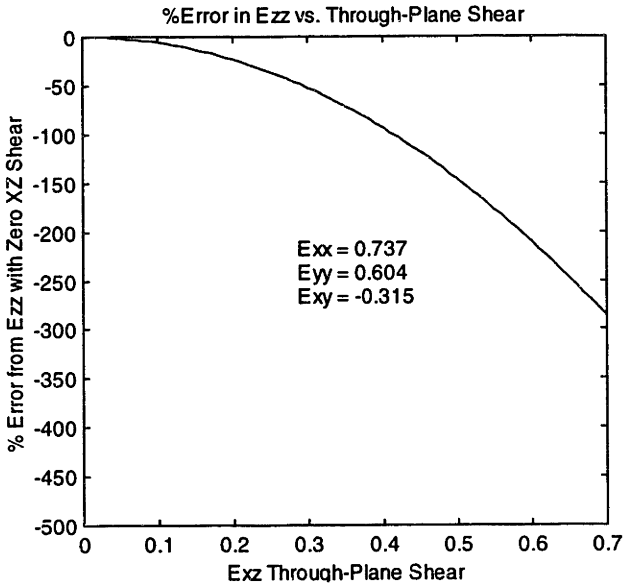

Element 30'

Figure 21 - Results of through-plane shear sensitivity study

4 Structure and Function in the Tongue

This thesis deals with the interrelation of tongue physiology with its myoarchitecture. The tongue musculature comprises an interwoven mesh whose physiology is difficult to predict *a priori*, whereas experimental physiology alone is not an adequate predictor of underlying myofiber contractions. This thesis aims to provide a comprehensive investigation of both physiological strain patterns, as well as the myoarchitectural effectors that produced this strain.

4.1.1 Discussion: Tongue Myoarchitecture

The myoarchitecture of the bovine tongue was explored with diffusion tensor magnetic resonance imaging. This technique capitalized on the inherent anisotropic diffusivity of myofibers to provide a virtual anatomical atlas of the tongue. While diffusion tensor MRI was successful in subdividing the tongue into distinct structural regions, a consideration of past histological and conventional dissection investigations provides an extending analysis and critique of this MRI method.

The anterior intrinsic core contains interdigitating populations of fibers (the transversus and verticalis), thus the sampled voxel was represented by a diffusion tensor comprising the sum proton diffusivity in each of the two distinct fiber populations. This is commonly referred to as the "partial volume effect." When a voxel contains a comparable quantity of each fiber population, the color-coded eigenvector may belong to either population; although, the diffusivity must be slightly greater along one of these two fiber directions. Thus, the anterior core region contained octahedra color coded *either* green or red, depending on which fiber population was locally more prevalent. In fact, this region was best appreciated by the anisotropy index, presented in section 2.4.

It should also be noted that the determination of the muscle orientation required the use of both color-coding of the principal eigenvector direction as well as three-dimensional graphics, since the colors of the color-sphere did not correspond to unique three-dimensional orientations. This condition resulted from the insensitivity of this color code to the relative signs of vector components. For example, the genioglossus and hyoglossus muscles are both coded blue-green although they have different three-

dimensional orientations, postero-superior in the sagittal plane for the genioglossus and antero-superior for the hyoglossus (section 2.2).

Another issue with this technique was in the interpretation of regions with significant fiber population cross-weaving, as occurs in the tongue core. In a situation such as this, the principal eigenvector should have aligned with the most prevalent population; however, it would be erroneous to assume that the second eigenvector was aligned along the second most prevalent population. In other words, it would be erroneous to assume that the core was composed of fiber populations that were orthogonal on the scale of the voxel based on the characteristic orthogonality of the eigensystem coordinate reference frame (represented by the octahedron). Decoding the fiber direction of the second (or even third, or fourth...) most prevalent fiber population requires higher resolution *within* the voxel; a topic for further research.

Angular dispersion was investigated by visualizing the $\mathbf{v}_1$-$\mathbf{v}_2$ plane as the end caps of cylinder icon (section 2.3). The $\mathbf{v}_1$-$\mathbf{v}_2$ plane signified the plane containing the greatest fiber angle dispersion. That is, if a voxel encloses more than one distinct fiber populations, the two most prevalent populations are coplanar with the $\mathbf{v}_1$-$\mathbf{v}_2$ plane. This property is useful when using cylinders to represent the diffusion tensor in cross-woven fiber regions, such as the anterior tongue core. In this region, fiber orientations were most dispersed, or varied, in the axial plane of the tongue. Thus, the two most prevalent fiber populations exist in this plane. However, it must be noted that the cylinder dispersion visualization technique cannot specify the direction of the most prevalent fiber population, and thus is most useful when at least two known populations are present.

4.1.2 Discussion: Tongue Protrusion and Bending

Tagging MRI was utilized to investigate the *in-vivo* muscular strain in the human tongue. The analysis provided a biomechanical basis for understanding the effect of local muscular activity on the physiological function of the tongue, and proposed a general model relating local contraction and tissue deformation in muscular hydrostats.

The results demonstrated the manner in which regional activation of the intrinsic musculature results in protrusive and bending motions. In anterior tongue protrusion, bi-directional contraction of mutually orthogonal intrinsic muscle fibers residing in the core

of the tongue resulted in protrusion along the tongue's longitudinal axis. This result was consistent with the tongue's role as a muscular hydrostat adhering to the isochoric condition (incompressibility), which specified that original volume was maintained throughout deformation. Contraction in the tongue core occurred in the superior-inferior and medial-lateral directions, consistent anatomically with the region's fiber orientation. This assumed that the x-y-z coordinate system of the image coincided with the anterior-superior-lateral coordinate system of the tongue, which was deemed reasonable from tagged images of the undeformed tissue. For this simple prototypical motion, negative strain presented in these directions was considered synonymous with muscle contraction because overlapping extrinsic muscle attachments lateral or superior to the regions in question were nonexistent. Such attachments could introduce compressive strain to uncontracted muscle tissue by deforming adjacent muscle fibers in the organ.

Anterior-posterior positive strain peaking at 218% was typical for the group studied and exemplified the notable expansive ability of the tongue tissue. The principal axis of tissue expansion was confirmed by visualization of the strain tensors (Figure 10c), which demonstrated that the major axis of octahedra in the anterior tongue coincided with the longitudinal axis of the organ; as would be expected for tongue protrusion. Furthermore, the absence of significant strain in the posterior and inferior portions of the organ refutes the hypothesis that the genioglossus muscle is responsible for anterior protrusion (Abd-el-Malek, 1955; Scardella *et al*, 1993). Interestingly, the region of positive superior-inferior strain (peaking at 0.472) observed in Figure 10e was due to the tongue body stretching slightly superior when extruding from the mouth.

Bending of the tongue, either upward or lateral, was caused by unilateral contraction of the longitudinal sheath combined with regional contraction of the core fibers. Contraction of the longitudinal muscle fibers on the side of the tongue closest to the center of curvature was demonstrated by the existence of negative strain values at the inside edge (Figures 14 and 15). These results thus supported the prediction made by Smith and Kier (1989), who proposed that unilateral contraction of the peripherally located and longitudinally oriented sheath was a mechanism for bending in a muscular hydrostat. The data additionally demonstrated a synergistic mechanism for tissue bending through graded core fiber contraction as a function of radial distance from the center of

curvature (Figure 11f, Figure 13f). Notably, some subjects exhibited graded contraction as a summed response of medial-lateral *and* superior-inferior fibers. This graded contraction resulted in a commensurate expansion in the antero-posterior direction that increased with distance from the center of curvature (Figure 11d, Figure 13e), thereby efficiently supplementing the contraction of the longitudinal sheath in the production of bending. The positive relationship between antero-posterior strain and distance from center of curvature appeared linear, thus justifying the use of a linear correlation coefficient. Similar to tongue protrusion, the region of positive superior-inferior strain seen in the sagittal bending image (Figure 11e) resulted from the tongue body being stretched superiorly toward the hard palate. Furthermore, the inactivity observed in the posterior and inferior portions of the tongue (Figure 11f) support the absence of genioglossus contraction in sagittal tongue bending. While neither tongue bending nor tongue protrusion manifested a significant contribution of the genioglossus muscle, this does not exclude a role of this muscle in more complex motor tasks, such as human speech or swallowing, in which the physiological demands for tissue versatility are greater. The absence of strain in the posterior portion of the tongue suggests that the styloglossus and hyoglossus muscles were also inactive during protrusion and bending. Since these muscles insert into the lateral aspects of the tongue body (and hence were not directly imaged in this study), the contraction of these muscles should manifest strain in the mid-sagittal slice by passive drag. Thus, the overall absence of strain in the posterior tongue, as was calculated by the analysis, leads to the conclusion that the extrinsic musculature was inactive for the motions studied.

Lingual contraction during bending resulted both in deformation and the skeletal support for that deformation. Hypothetically, if tongue bending were associated only with unilateral contraction of the longitudinal sheath, the tissue response would be longitudinal shortening. This behavior has been depicted in the form of an idealized beam (Figure 22).

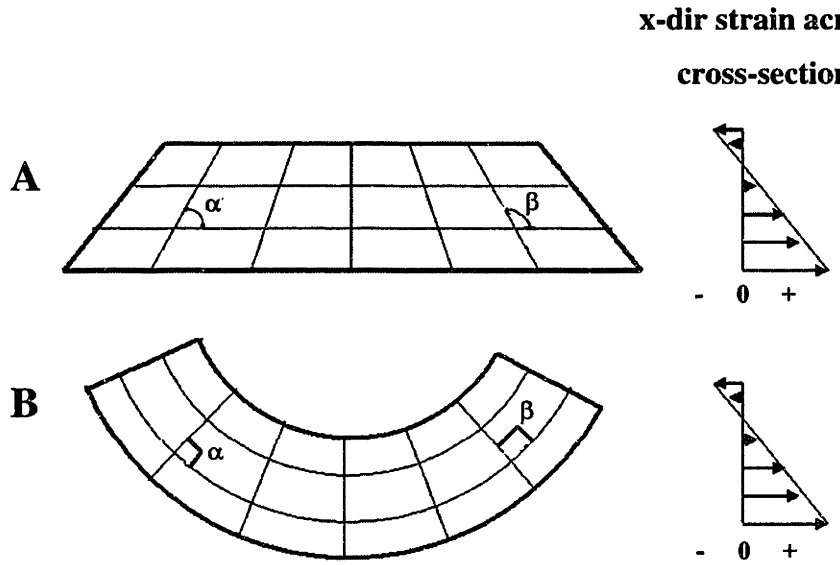

Figure 22 - Idealized deformed beams: (A) a beam with little resistance to shear and (B) a beam undergoing shear-free deformation.

While both deformed contours exhibit the same x-direction normal strain across their cross-sections, beam A does not resist shear since angles α and β deviate from the undeformed value of 90° (Figure 22a). Hence, the left portion of the beam is subjected to positive (clockwise) shear, while the right is subjected to negative (counter-clockwise) shear. On the other hand, beam B is completely devoid of shear strain since α and β remain right angles, thus defining pure bending (Figure 22b).

The data indicate that sagittal tongue bending was a compromise between these two idealizations. Pure tongue bending was superimposed upon the shear deformation exhibited by the right portion of beam A (Figure 22a). The existence of negative shear (Figure 12) resulted from the inferior constraint imposed by the uncontracted genioglossus muscle. Due to the close anatomical relationship between the intrinsic and extrinsic muscle groups, shear strain is necessarily introduced when tissue expansion (as seen in the intrinsic core fibers) occurs adjacent to an uncontracted muscle (such as the genioglossus fibers inferior to the intrinsic core). Furthermore, the amount of shear strain produced when the intrinsic musculature contracts to impose x-direction normal strain will depend on the shear modulus (modulus of rigidity) of the tissue. The greater the

shear modulus, G, the lower will be the shear strain. In order to resist shear during bending, the core fibers must contract, thus increasing the shear modulus for the tissue by increasing muscle tone, simulating skeletal support.

In order to extend the two-dimensional strain analysis of single shot tagging MRI, it was assumed that the tongue muscle tissue was incompressible, and hence isochoric. Mathematically, this means that the determinant of the deformation gradient tensor is equal to unity. This one equation can be solved for its one unknown (E_{zz}, through-plane axial strain) if it is assumed that the through-plane shear strains, E_{xz} and E_{yz}, are negligible. For tongue motions that are symmetric with respect to the imaging plane, this assumption was likely to be valid; however, tongue motions asymmetric to the imaging plane are likely to introduce through-plane shears, which cannot be measured, and may therefore invalidate this assumption

This methodology was inherently dependent upon the presence of adequate tag contrast. Tag fading, i.e. loss of contrast between tagged and untagged tissue, can result from one of several causes, namely T_1 decay of the tagged tissue's longitudinal magnetization, motion artifact, and through-plane motion. T_1 decay is an intrinsic tissue property, and therefore served to limit the TI time between tagging and imaging. Blurring of the tags may also result if physiological tissue motion is substantial during the imaging time, whether this motion was within the imaging slice or "through-plane." Blurring or fading of the tags decreases the contrast between tagged and untagged tissue, potentially making the grid unrecoverable. Thus, minimizing imaging time is important for mitigating motion artifact.

4.1.3 Discussion: Swallowing

The tongue is a muscular organ, which is instrumental in the manipulation, configuration, and delivery of the ingested bolus from the oral cavity to the oropharynx during swallowing. These functions are carried out through a series of characteristic deformations, which are designed to first control (early and late accommodation) and then rapidly propel the bolus (propulsion). In order to determine the intramural dynamics of the lingual musculature associated with these deformations, tagging magnetic

resonance imaging was used to quantify local muscle deformation (i.e. strain) in relation to overall tissue shape.

Early accommodation was characterized by the containment of the bolus in a grooved depression at the middle portion of the tongue's dorsal surface. This grooved depression appeared to have been created by a synergistic contraction of the anterior genioglossus in concert with the hyoglossus, verticalis (intrinsic), and transversus (intrinsic) muscles. Verticalis contraction was seen as a region of negative y-direction strain in the anterior tongue (Figure 16d), resulting in x-direction expansion of the tongue tip toward the incisors. Transversus contraction was suggested on the basis of subtle z-direction negative strain (Figure 16e). There was, however, strong evidence of negative y-direction strain directly below the bolus, producing a depression of the containing groove. This tissue contraction could be the direct result of genioglossus contraction, or could have been caused through passive drag by contraction of the hyoglossus, which inserts into the mid-portion of the tongue body, laterally from below (hence not visualized in the mid-sagittal slice). Genioglossus contraction in the swallow has been demonstrated by previous EMG studies (Miyawaki *et al*, 1975); whereas, synergistic involvement of the hyoglossus could be inferred from the strain tensor visualization map (Figure 16c). This strain map demonstrated that the contractile eigenvectors (visualized as the short axes of octahedra - the direction of greatest contractile strain when z-direction strain is positive) were oriented postero-inferiorly. Since the mid-sagittal slice is directly medial to the lateral insertions of the hyoglossus, this strain pattern was consistent with either genioglossus or hyoglossus contraction, occurring independently or in concert. These contractions were associated with x and z-direction expansion in this region, elongating the grooved depression and improving bolus containment. X-direction expansion in the posterior tongue aided in closing off the oropharynx.

Late accommodation was characterized by a shifting of the bolus toward the posterior dorsal surface of the tongue, in effect, "priming the lingual pump" before eventual propulsion into the oropharynx. The soft palate was shifted superiorly, thus closing off the nasopharynx. The most prominent finding during this phase was an increase of negative y-direction strain (i.e. inferior-directed contraction) in the posterior region of the tongue, which contained the bolus. This contraction is responsible both for the creation of

the posterior depression, and for the extension of the bolus depression in the x and z directions (due to tissue incompressibility). The extent to which these contractions are due to activity of the posterior fibers of the genioglossus or to passive drag secondary to hyoglossus contraction cannot be conclusively determined from these data. The genioglossus fans out into the mid-sagittal slice from its attachment on the mandible and would present octahedral short axes oriented anterior-inferiorly. In contrast the hyoglossus enters the mid-posterior tongue at its lateral aspect from its attachment on the hyoid bone and would present octahedral short axes oriented posterior-inferiorly. Conceivably, the degree to which these muscles contribute to the accommodating depression in the posterior tongue may also vary as a function of bolus volume or viscosity, or as a function of pathological regulation of tongue contractility. Translation of the contractile region from the anterior to the posterior genioglossus (early to late accommodation) transferred the bolus retrograde via the grooved depression, preparing the bolus for propulsion.

Bolus propulsion was characterized by the retrograde motion of the tongue toward the pharyngeal wall, thus expelling the cradled bolus from the oral cavity. The most prominent effect was on the posterior tongue, with significant expansion of the tissue in the x and y directions and concomitant z direction contraction. The styloglossus, which inserts into the posterior tongue body on its lateral aspects and is directed postero-superiorly towards its attachment point on the styloid process, most likely produced this universally observed strain pattern by passively dragging the tissue in the tongue's mid-sagittal slice. This mechanism was supplemented by contraction of intrinsic transversus muscle fibers, which are also located in the posterior tongue. This contraction would cause tissue expansion in the x and y directions due to incompressibility of the tongue tissue. Octahedra in the posterior tongue had their principal eigenvector (octahedral long axis), or the direction of greatest expansion, oriented in a postero-superior direction. Sole contraction of the styloglossus (in a postero-superior direction) could not produce expansive strain *above* its insertion point, in the mid-portion of the tongue's lateral surfaces since the tongue is constrained from below. Thus, styloglossus contraction would stretch the tongue tissue located between its insertion point and the tongue's inferior attachment. Because postero-superior expansion in the posterior tongue was seen

to exist all the way to the dorsal surface, a synergistic mechanism must be at work. This effect could only come from contraction of the z-directed transversus muscle in this portion of the tongue.

Axial strain values were reported as the mean of all elements in a given region across all subjects (Table 1), as well as peak values in a given region for a representative subject (Figures 16-18). While the former technique sufficiently mitigates spurious digitization errors, accounts for inter-subject variability, and provides a datum for gross activity in the region, the result may not differentiate two distinct contractile regions or contraction of only a portion of the muscle, such as localized genioglossus contraction of specific motor units. Conversely, the latter technique of reporting maximum and minimum peak values could potentially differentiate localized muscle function (at the resolution of the element), however it is highly sensitive to digitization error.

Since the imaging technique was inherently two-dimensional, the calculation of axial strain in the through-plane direction (at right angles to the sagittal imaging plane) required two assumptions: 1) The tissue maintained a constant volume with deformation, i.e. incompressibility condition, and 2) through-plane shear strain was negligible. The latter condition is valid for tongue motions, which are symmetric about the midline sagittal plane, as was the case for normal swallows. However, these assumptions may not be valid under pathological conditions in which one region of the tongue is asymmetrically affected, such as stroke or muscular tissue injury. The application of tagging MRI in these settings may thus require accurate gating of MR imaging to swallow onset, thereby significantly lowering imaging time and permitting the application of the technique along asymmetric slices without significant motion artifact.

These data were consistent with a biomechanical model in which the intrinsic and extrinsic fibers function synergistically rather than as independent actuators. In this regard, the unique myoarchitecture of the tongue allows the organ to function efficiently as a muscular hydrostat (Smith and Kier, 1989); a term whose properties include 1) tissue incompressibility derived from a highly aqueous composition and 2) the ability to elicit tissue deformation while simultaneously providing skeletal support for that tissue. The former is evidenced by contracting lingual myofibers, which induce tissue compression along fiber directions and tissue expansion along directions orthogonal to the fibers (due

to tissue incompressibility). In both accommodation and propulsion, physiologic function was performed though a synergistic combination of tissue compression and expansion. In fact, tissue incompressibility necessitates the simultaneous existence of both compression and expansion for a given tissue element, while the tongue's interdigitating myofibers insure that compression/expansion coupling synergistically produces the intended function. Conceivably, deglutitive function in patients with oral phase dysphagia may be impaired through a pathological reorganization of the underlying myoarchitecture, and the concomitant alteration of this compression/expansion distribution.

5 Conclusion

The tongue is an organ whose physiology is closely linked to its myoarchitecture, thus necessitating an integrated approach considering both functional deformation as well as the underlying anatomical geometry. Magnetic resonance imaging techniques were used to successfully complete both of these investigations and provided insight into the biomechanics of tongue deformation.

Ultimately, the myoarchitecture of an *in-vivo* deforming human tongue needs to be resolved in order to perform a comprehensive biomechanical analysis, incorporating both structure and function. Diffusion tensor MRI successfully produced a virtual anatomical atlas of an *ex-vivo* bovine specimen, constituting an important step towards this goal. Furthermore, future modeling endeavors, such as finite element modeling, could incorporate diffusion tensor MRI to derive functional geometry. FEM must include active stress generation within the modeled continuum. The directional characteristics of this stress generation could be elucidated by diffusion tensor MRI, which also treats the tissue as a continuum, deriving myofiber and hence contractility orientation within the tissue. Discrete contractile patterns with this model could then be tweaked until the physiological strain pattern within the mid-sagittal slice converged to the pattern observed with empirical techniques (such as tagging MRI), potentially providing a validation for the theoretical model - a necessary precursor for modeling normal physiological variability and pathophysiology.

This thesis also employed tagging MRI as a non-invasive experimental technique to resolve *in-vivo* physiological strain patterns within the tongue. Tagging MRI proved useful for investigating anterior protrusion, and sagittal and lateral bending. Specific intrinsic and extrinsic muscle contraction patterns were then proposed based on the 3D strain maps they would effectively produce. These results have defined the underlying mechanical mechanisms for tongue protrusion and bending, prototypical motions for the more complex activities associated with speech and swallowing. Furthermore, the results provided evidence that the tongue has the ability to produce deformation as well as providing skeletal support for that deformation, thus confirming the characterization of this organ as a muscular hydrostat. Another application of the tagging MRI technique was

to investigate intramural muscle mechanics for the tongue during normal swallowing. Tagging MRI provided evidence for a synergistic mechanical model involving both the intrinsic and extrinsic muscles during this complex physiological tissue deformation.

Appendix

The following is a derivation of the equations for the non-linear Green's strain tensor components.

Consider the general deforming body defined by two perpendicular line elements:

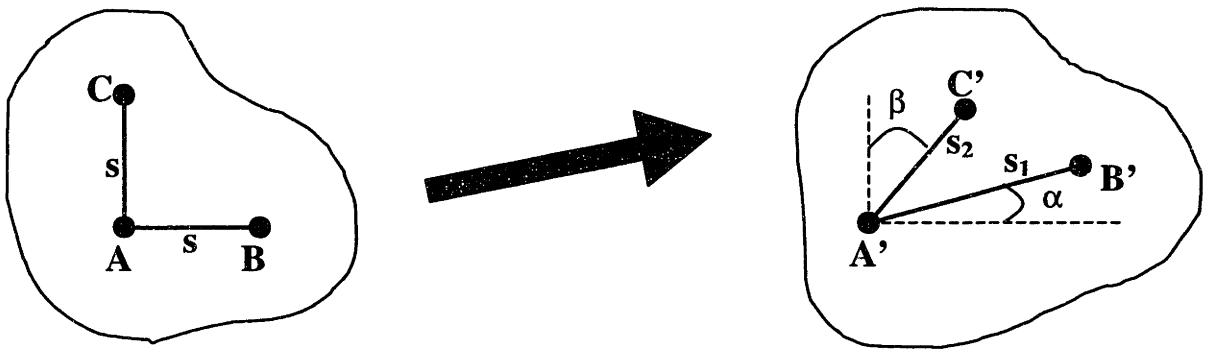

Figure A.1 - Two perpendicular line elements describing a general deforming body

The deformation gradient, **F**, transforms any line element dX to dx.

$$dx = \mathbf{F}dX \tag{A.1.0}$$

By the polar decomposition theorem, the deformation gradient can be decomposed into an orthogonal rotation tensor, **R**, and a symmetric, positive-definite right stretch tensor **U**.

$$\mathbf{F} = \mathbf{RU} \tag{A.2.0}$$

Thus, assume a resting 3D orthogonal Cartesian coordinate system defined by the unit vectors e_x, e_y, e_z with

$$\overrightarrow{AB} = s\,e_x \tag{A.3.0}$$

$$\overrightarrow{AC} = s\,e_y \tag{A.3.1}$$

and deformed line elements defined by

$$\overrightarrow{A'B'} = \mathbf{F}\overrightarrow{AB} = s\mathbf{F}e_x \tag{A.4.0}$$

$$\overrightarrow{A'C'} = \mathbf{F}\overrightarrow{AC} = s\mathbf{F}e_y \tag{A.4.1}$$

Hence, since the rotation tensor does not cause any stretch, the deformed line element lengths are given by the following formulae:

$$s_1 = |\mathrm{A'B'}| = s|\mathbf{F}e_x| = s|\mathbf{U}e_x| \tag{A.5.0}$$

$$s_2 = |\mathrm{A'C'}| = s|\mathbf{F}e_y| = s|\mathbf{U}e_y| \tag{A.5.1}$$

Also, the relative angle between the two deformed line elements can be given by

$$\overrightarrow{A'B'} \bullet \overrightarrow{A'C'} = s^2\, \mathbf{F}e_x \bullet \mathbf{F}e_y = s_1 s_2 \cos(\pi/2 - \phi)$$

or

$$s^2\, \mathbf{U}e_x \bullet \mathbf{U}e_y = s_1 s_2 \sin\phi$$

hence

$$\mathbf{U}e_x \bullet \mathbf{U}e_y = \frac{s_1 s_2}{s^2}\sin\phi \tag{A.5.2}$$

The general definition of a Lagrangian strain tensor is

$$\mathbf{E}_{\text{Lagrangian}} = \frac{1}{m}\left(\mathbf{U}^m - \mathbf{I}\right) \tag{A.6.0}$$

where $m \neq 0$ is a scalar. By definition (Chandrasekharaiah, 1994; Lai, 1993), Green's non-linear strain tensor is given by the special case, m=2.

$$\mathbf{E}_{\text{Green}} = \frac{1}{2}\left(\mathbf{U}^2 - \mathbf{I}\right) \tag{A.6.1}$$

Finally, the elements of this strain tensor can be derived by incorporating equations (A.5.0-2) with the definition given in (A.6.1).

$$\begin{aligned} E_{xx} &= \mathbf{E}e_x \bullet e_x = \frac{1}{2}\left(\mathbf{U}^2 - \mathbf{I}\right)e_x \bullet e_x \\ &= \frac{1}{2}\left(\mathbf{U}^2 e_x \bullet e_x - 1\right) = \frac{1}{2}\left(\mathbf{U}e_x \bullet \mathbf{U}e_x - 1\right) \\ &= \frac{1}{2}\left(\left|\mathbf{U}e_x\right|^2 - 1\right) \\ &= \frac{1}{2}\left(\frac{s_1^2}{s^2} - 1\right) \end{aligned} \tag{A.7.0}$$

$$\begin{aligned} E_{yy} &= \mathbf{E}e_y \bullet e_y = \frac{1}{2}\left(\mathbf{U}^2 - \mathbf{I}\right)e_y \bullet e_y \\ &= \frac{1}{2}\left(\mathbf{U}^2 e_y \bullet e_y - 1\right) = \frac{1}{2}\left(\mathbf{U}e_y \bullet \mathbf{U}e_y - 1\right) \\ &= \frac{1}{2}\left(\left|\mathbf{U}e_y\right|^2 - 1\right) \\ &= \frac{1}{2}\left(\frac{s_2^2}{s^2} - 1\right) \end{aligned} \tag{A.7.1}$$

$$E_{xy} = \mathbf{E}e_y \bullet e_x = \frac{1}{2}\left(\mathbf{U}^2 - \mathbf{I}\right)e_y \bullet e_x$$
$$= \frac{1}{2}\mathbf{U}^2 e_y \bullet e_x = \frac{1}{2}\mathbf{U}e_x \bullet \mathbf{U}e_y$$
$$= \frac{s_1 s_2}{2s^2}\sin\phi \qquad \text{(A.7.2)}$$

These definitions provide a complete 2-Dimensional description of the strain state. A 3-dimensional extension of the data can also be provided if the tissue is assumed to be incompressible. Then, element volume is isochoric, and the third principal strain can be found from the determinant of the deformation gradient and definition (A.6.1). Here E_{11} and E_{22} are the principal strains in the x-y plane.

Incompressibility requires that det**F**=1. Because of (A.2.0) and the orthogonality of the rotation tensor **R**, this implies that det$\mathbf{U}^2$=1. Consequently by (A.6.1),

$$\Rightarrow \det\left(2\mathbf{E} + \mathbf{I}\right) = 1$$

$$\det\begin{pmatrix} 2E_{11}+1 & 0 & 0 \\ 0 & 2E_{22}+1 & 0 \\ 0 & 0 & 2E_{33}+1 \end{pmatrix} = 1$$

$$\Rightarrow (1+2E_{11})(1+2E_{22})(1+2E_{33}) = 1$$

$$E_{33} = \frac{1}{2}\left[\frac{1}{(1+2E_{11})(1+2E_{22})} - 1\right] \qquad \text{(A.8.0)}$$

If the out-of-tagging-plane shear strains (E_{xz} and E_{yz}) are negligible, $E_{zz} = E_{33}$, and the orientation of the third eigenvector is coincident with the z-axis. Hence, the strain state can be completely defined in the x-y-z Cartesian coordinate system.

Bibliography

1. Abd-el-Malek, S. (1955) The part played by the tongue in mastication and deglutition. *Journal of Anatomy* **89**, 250-254.

2. Axel, L., Dougherty, L. (1989) MR Imaging of Motion with Spatial Modulation of Magnetization. *Radiology* **171**, 841-845.

3. Azhari, H., Weiss, J., Rogers, W., Siu, C., Zerhouni, E., Shapiro, E. (1993) Noninvasive quantification of principal strains in normal canine hearts using tagged MRI images in 3-D. *American Journal of Physiology* **264**, H205-H216.

4. Basser, P., Mattiello, J., LeBihan D. (1994) MR Diffusion Tensor Spectroscopy and Imaging. *Biophysical Journal* **66**, 259-267.

5. Bloch, F. (1946) Nuclear Induction. *Physical Reviews* **70**, 460-474.

6. Chandrasekharaiah, D., Debnath, L. (1994) *Continuum Mechanics*. 188-190. Academic Press.

7. Chiel, H., Crago, P., Mansour, J., Hathi, K. (1992) Biomechanics of a muscular hydrostat: a model of lapping by a reptilian tongue. *Biological Cybernetics* **67**, 403-415.

8. Cook IJ, Dodds WJ, Dantas RO, Kern MK, Massey BT, Shaker R, Hogan WJ. (1989) Timing of videofluoroscopic, manometric events, and bolus transit during the oral and pharyngeal phases of swallowing. *Dysphagia* **4**, 8-15.

9. Dantas RO, Kern MK, Massey BT, Dodds WJ, Kahrilas PJ, Brasseur JG, Cook IJ, Lang IM. (1990) Effect of swallowed bolus variables on oral and pharyngeal phases of swallowing. *American Journal of Physiology* **258**: G675-681.

10. Devgan, B., Gross, C., McCloy, R., Smith, C. (1978) Anatomic and physiologic aspects of sword swallowing. *Ear, Nose, and Throat Journal* **57**, 58-66.

11. Doble, E., Leiter, J., Knuth, S., Daubenspeck, J., Bartlett jr., D. (1985) A noninvasive intraoral electromyographic electrode for genioglossus muscle. *Journal of Applied Physiology* **58**(4), 1378-1382.

12. Dodds WJ, Stewart ET, Logemann JA. (1990) Physiology and radiology of the normal oral and pharyngeal phases of swallowing. *American Journal of Radiology* **154**, 953-963.

13. Drace, J.E., Pelc, N.J. (1994) Skeletal Muscle Contraction: Analysis with Use of Velocity Distributions from Phase-Contrast MR Imaging. *Radiology* **193**, 423-429.

14. Elliott, G.F., Lowy, J., Worthington, C.R. (1963) An X-ray and light diffraction study of the filament lattice of striated muscle in the living state and in rigor. *Journal of Molecular Biology* **6**, 295-305.

15. Gilbert R.J., Daftary, S., Campbell, T.A., Weisskoff, R.M. (1997) Patterns of lingual deformation associated with bolus containment and propulsion during deglutition as determined by echoplanar magnetic resonance imaging. *Journal of Magnetic Resonance Imaging* (in press).

16. Groher, M. (1997) *Dysphagia: Diagnosis and Management*. Butterworth-Heinemann, 3rd ed.

17. Hamlet SL, Stone M, Shawker TH. (1988) Posterior tongue grooving in deglutition and speech: Preliminary observations. *Dysphagia* **3**, 65-68.

18. Hashimoto, K., Suga, S. (1986) Estimation of the muscular tensions of the human tongue by using a three-dimensional model of the tongue. *Journal of the Acoustical Society of Japan* (E) **7**, 39-46.

19. Hiiemae, K., and Crompton, A. (1985) Mastication, food transport and swallowing. In *Functional Vertebrate Morphology*, eds. M. Hildebrand, D. M. Bramble, K. F. Liem, and D. B. Wake, pp. 262-90. Belknap Press.

20. Kahrilas, P.J., Lin, S., Logemann, J.A., Ergun, G.A., Facchini, F. (1993) Deglutitive tongue action: volume accommodation and bolus propulsion. *Gastroenterology* **104**, 152-162.

21. Kahrilas PJ, Logemann JA, Lin S, Ergun GA. (1992) Pharyngeal clearance during swallowing: a combined manometric and videofluoroscopic study. *Gastroenterology* **103**, 128-136.

22. Krol, R., Knuth, S., Bartlett jr., D. (1984) Selective reduction of genioglossal muscle activity by alcohol in normal human subjects. *American Review of Respiratory Disease* **129**, 247-250.

23. Lai, W.M., Rubin, D., Krempl, E. (1993) *Introduction to Continuum Mechanics*. Pergamon Press, 3rd ed.

24. Miller, A.J. (1982) Deglutition. *Physiological Reviews* **62**:1, 129-184.

25. Miyawaki, K. (1974) A study of the musculature of the human tongue. *Annual Bulletin of the Research Institute of Logopedics and Phoniatrics - University of Tokyo* **8**, 23-50.

26. Miyawaki K., Hirose H., Ushijima T., Sawashima M. (1975) A preliminary report on the electromyographic study of the activity of lingual muscles. *Annual Bulletin of the Research Institute of Logopedics and Phoniatrics - University of Tokyo* **9**, 91-106.

27. Moulton, M. J., Creswell, L., Downing, S., Actis, R., Szabo, B., Vannier, M., and Pasque, M. (1996) Spline surface interpolation for calculating 3-D ventricular strains from MRI tissue tagging. *American Journal of Physiology* **39**, H281-H297.

28. Niitsu, M., Kumada, M., Campeau, N.G., Niimi, S., Riederer, S.J., Itai, Y. (1994) Tongue displacement: visualization with rapid tagged magnetization-prepared MR Imaging. *Radiology* **191**, 578-580.

29. Norris, D., Niendorf, T. (1995) Interpretation of DW-NMR Data: dependence on experimental conditions. *NMR in Biomedicine* **8**, 280-288.

30. Pierpaoli, C., Basser, P.J. (1996) Toward a quantitative assessment of diffusion anisotropy. *Magnetic Resonance in Medicine* **36**: 893-906.

31. Pouderoux, P., Kahrilas, P. (1995) Deglutitive tongue force modulation by volition, volume, and viscosity in humans. *Gastroenterology* **108**, 1418-1426.

32. Sanguineti, V., Laboissiere, R., Payan, Y. (1997) A control model of human tongue movements in speech. *Biological Cybernetics* **77**(1), 11-22.

33. Sauerland, E., Harper, R. (1976) The human tongue during sleep: electromyographic activity of the genioglossus muscle. *Experimental Neurology* **51**, 160-170.

34. Scardella, A., Krawciw, N., Petrozzino, J., Co, M., Santiago, T., Edelman, N. (1993) Strength and endurance characteristics of the normal human genioglossus. *American Review of Respiratory Disease* **148**, 179-184.

35. Shawker TH, Sonies BC, Stone M. (1984) Sonography of speech and swallowing. In *Ultrasound Annual*, eds. R.C. Sanders, M.C. Hill, pp. 237-260. New York: Raven.

36. Smith, K.K. (1984) The use of the tongue and hyoid apparatus during feeding in lizards (*Ctenosaura similis and Tupinambis nigropunctatus*). *Journal of Zoology London* **202**, 115-143.

37. Smith, K.K. (1986) Morphology and function of the tongue and hyoid apparatus in *Varanus* (Varanidae, Lacertilia). *Journal of Morphology* **187**, 261-287.

38. Smith, K.K., Kier, W.M. (1989) Trunks, tongues, and tentacles: moving with skeletons of muscle. *American Scientist* **77**, 29-35.

39. Stone M. (1990) A three-dimensional model of tongue movement based on ultrasound and x-ray microbeam data. *Journal of the Acoustical Society of America* **87**, 2207-2217.

40. Wedeen, V.J. (1992) Magnetic resonance imaging of myocardial kinematics. *Magnetic Resonance in Medicine* **27**, 52-67.

41. Wein, B., Bockler, R., Klajman, S. (1991) Temporal reconstruction of sonographic imaging of disturbed tongue movements. *Dysphagia* **6**, 135-139.

42. Wilhelms-Tricarico, R. (1995) Physiological modeling of speech production: Methods for modeling soft-tissue articulators. *Journal of the Acoustic Society of America* **97** (5), 3085-3098.

43. Young, A. A., Axel, L. (1992) Three-dimensional Motion and Deformation of the Heart Wall: Estimation with Spatial Modulation of Magnetization - A Model based Approach. *Radiology* **185**, 241-247.

44. Young, A. A., Axel, L., Dougherty, L., Bogen, D.K., and Parenteau, C. S. (1993) Validation of tagging with MR imaging to estimate material deformation. *Radiology* **188**, 101-108.

45. Zerhouni, E.A., Parish, D.M., Rogers, W., Yang, A., Shapiro, E.P. (1988) Human heart: tagging with MR imaging - a method for noninvasive assessment of myocardial motion. *Radiology* **169**, 59-63.

THESIS PROCESSING SLIP

FIXED FIELD: ill. _____ name _____

index _____ biblio _____

▶ COPIES: (Archives) Aero Dewey (Eng) Hum

Lindgren Music Rotch Science

TITLE VARIES: ▶ ☐ _____

NAME VARIES: ▶ ☒ Joseph

IMPRINT: (COPYRIGHT) _____

▶ COLLATION: 80 p.

▶ ADD: DEGREE: _____ ▶ DEPT.: _____

SUPERVISORS: _____

NOTES:

cat'r: date:

page: 1133

▶ DEPT: M.E.

▶ YEAR: 1998 ▶ DEGREE: ~~B.S.~~ S.M.

▶ NAME: NAPADOW, Vitaly J.